SETD2 is required for DNA double-strand break repair and activation of the p53-mediated checkpoint

Sílvia Carvalho[1], Alexandra C. Vítor[1], Sreerama Chaitanya Sridhara, Filipa B. Martins, Ana C. Raposo, Joana M. P. Desterro, João Ferreira & Sérgio Fernandes de Almeida*

Instituto de Medicina Molecular, Faculdade de Medicina da Universidade de Lisboa, Portugal

[1] These authors contributed equally to this work.

* Corresponding author

Mailing address: SAlmeida Unit, Instituto de Medicina Molecular, Faculdade de Medicina

Av. Prof. Egas Moniz, 1649-028 Lisboa, Portugal

Fax: +351 21 7999504 Phone: +351 21 7999505

sergioalmeida@fm.ul.pt

Running title: SETD2 is necessary for DNA repair

Abstract

Histone modifications establish the chromatin states that coordinate the DNA damage response. Here, we show that SETD2, the enzyme that trimethylates histone H3 lysine 36 (H3K36me3), is required for ATM activation upon DNA double-strand breaks (DSBs). Moreover, we find that SETD2 is necessary for homologous recombination repair of DSBs by promoting the formation of RAD51 presynaptic filaments. In agreement, SETD2-mutant clear cell renal cell carcinoma (ccRCC) cells displayed impaired DNA damage signaling. However, despite the persistence of DNA lesions, SETD2-deficient cells failed to activate p53, a master guardian of the genome rarely mutated in ccRCC and showed decreased cell survival after DNA damage. We propose that this novel SETD2-dependent role provides a chromatin bookmarking instrument that facilitates signaling and repair of DSBs. In ccRCC, loss of SETD2 may afford an alternative mechanism for the inactivation of the p53-mediated checkpoint without the need for additional genetic mutations in TP53.

Introduction

DNA double-strand breaks (DSBs) are the most catastrophic form of DNA damage and pose great threat to genome stability. The major sensor of DSBs is ataxia telangiectasia mutated (ATM) kinase, which is critical for the initial steps of the DNA damage response (DDR). In response to DSBs, ATM phosphorylates and regulates the activity of several substrates involved in DNA repair, such as p53-binding protein 1 (53BP1) and histone H2AX (Matsuoka et al, 2007). To effectively repair a DSB, mammalian cells can choose from two different DDR pathways: nonhomologous end-joining (NHEJ) and homologous recombination (HR) (Chapman et al, 2012). During NHEJ, the broken DNA ends are blocked from 5' end resection and held in close proximity by the Ku70-Ku80 heterodimer (Ku) (Lieber, 2010). HR is initiated when the 5' DNA ends are resected by nucleases and helicases, generating two 3' single-stranded DNA overhangs coated with phosphorylated replication protein A (RPA) that drives the formation of a RAD51 filament prior to strand invasion (Chapman et al, 2012). In contrast to NHEJ, which promotes direct ligation of the DSB ends in an error-prone manner and is available throughout the cell cycle, HR employs homologous sequences available after DNA replication as templates for error-free DNA repair (San Filippo et al, 2008). Both pathways proceed through a cascade of events whereby DNA damage sensors, transducers and effectors detect and rejoin the broken DNA ends (Harper & Elledge, 2007). All these events take place within the relatively restricted environment of chromatin, the nucleoprotein complex of histones and DNA assembled into nucleosomes. DNA damage challenges chromatin integrity by eliciting the destabilization and reorganization of its structure (Soria et al, 2012). Conversely, a strictly regulated set of post-translational modifications of the histones N-terminal tails regulates the recruitment and activation of DDR factors (Greenberg, 2011). The most studied response of histones to DNA damage is the phosphorylation of the histone variant H2AX, which serves as a molecular beacon that signals the presence of DNA damage (Rogakou et al, 1998). Phosphorylated H2AX (γH2AX) arises within minutes after DNA damage and has a key role in the recruitment of multiple DDR factors to the repair centers (Lukas et al, 2011). In addition to γH2AX, other histone modifications have been shown to play key roles during the DDR, illustrating the importance of a thorough characterization of the chromatin landscape of a DNA lesion. We have recently shown that the histone methyltransferase SETD2 (also termed KMT3 or HYPB), which is responsible for all H3K36

trimethylation, but not H3K36 mono- or dimethylation (Edmunds et al, 2008), acts as a determinant of chromatin integrity by regulating nucleosome dynamics during transcription (Carvalho et al, 2013). A role of H3K36me3 in maintaining chromatin integrity was recently disclosed by the finding that the DNA mismatch repair (MMR) protein MutSα binds H3K36me3 and that SETD2 is necessary for human DNA MMR, a mechanism that corrects mismatches generated during DNA replication (Li et al, 2013). Nevertheless, whether SETD2 impinges on the cell's ability to cope with DNA DSBs is not yet known. Here, we investigate the role of SETD2 on the cellular response to DNA DSBs. Our findings identify a novel role of this histone methyltransferase in rendering cells competent to repair DSBs. We demonstrate using powerful reporter assays that SETD2 is necessary for the DDR and that depletion of SETD2 impairs ATM activation and leads to delayed recruitment of 53BP1 to sites of DSBs. Our data further reveal that SETD2 is required for the recruitment of RAD51 to resected DNA 5' ends and SETD2-depleted cells show reduced homology-directed repair of DSBs.

SETD2 mutations were recently found in several cancers, such as clear cell renal cell carcinoma (ccRCC) (Dalgliesh et al, 2010; Duns et al, 2010; Fontebasso et al, 2013; Joseph et al, 2014; Varela et al, 2011; Zhang et al, 2012). In ccRCC the p53-mediated cell cycle checkpoint is frequently inactivated despite the fact that the *TP53* tumor suppressor gene is rarely mutated (Dalgliesh et al, 2010; Gurova et al, 2004; Sato et al, 2013). This puzzling observation suggests that the p53 signaling in ccRCC might be repressed by an alternative mechanism. Herein we further investigated whether the role of SETD2 in the DDR extends to the regulation of the p53-mediated checkpoint. We show that ccRCC cells carrying inactivating mutations on *SETD2* phenocopy the impaired DDR observed in *SETD2* RNAi-depleted human cells. Importantly, SETD2 inactivation severed the p53-dependent cell cycle checkpoint despite the persistence of unrepaired DNA lesions in ccRCC cells. We propose that this unprecedented role of SETD2 in the DDR constitutes a novel tumor suppressor mechanism that could explain the high frequency of *SETD2* mutations found in several cancers and may provide an alternative mechanism for evasion of the p53-mediated checkpoint in *TP53* wt ccRCC cells.

Results

SETD2 is necessary for the recruitment and activation of early DDR factors

To assay how SETD2 impinges on the cellular response to chemically induced DSBs, we monitored the DDR by measuring the dynamics of phosphorylation of the major DSB sensor ATM. Human Osteosarcoma (U2OS) cells were challenged with three different DNA-damaging agents: the topoisomerase II inhibitor etoposide, which is known to induce a large amount of DSBs (Burden et al, 1996) and the radiomimetic dsDNA-cleaving agents neocarzinostatin (NCS) (Goldberg, 1987) and phleomycin (Moore, 1988). We depleted *SETD2* mRNA by RNA interference (RNAi) using three different synthetic small interfering RNA duplexes, which resulted in a global loss of the H3K36me3 histone mark that persisted throughout the entire chase periods following the DNA damage (Figure 1A, B and C). As a control, we used the GL2 duplex, which targets firefly luciferase (Elbashir et al, 2001). In control cells, the levels of H3K36me3 remained constant during the DDR and were undistinguishable from those of undamaged cells, suggesting that this histone mark is not amplified following the DSBs (Figure 1A, B and C). Analysis of the phosphorylation levels of ATM revealed that the DDR was promptly activated upon induction of DSBs with the three compounds (Figure 1). ATM phosphorylation (pATM) peaked at the early time points after each treatment in control cells (Figure 1A, B and C). In contrast, SETD2-depleted cells revealed a significant impairment in DNA damage signaling as revealed by decreased pATM levels detected upon treatment with each of the three drugs (Figure 1A, B and C). In agreement with impaired ATM activation, the phosphorylation levels of its downstream substrates H2AX and 53BP1 decreased in SETD2-depleted cells following treatment with NCS or, more appreciably, etoposide (Figure 1A and B). In DSBs induced by phleomycin, depletion of SETD2 had only a very mild impact on phosphorylation of 53BP1 or H2AX (Figure 1C) suggesting that either the remaining pATM is sufficient to transduce the DNA damage signalling or that alternative ATM-independent pathways operate in phleomycin-induced DSBs.

To directly visualize how does ablation of SETD2 impinge on 53BP1 nucleation at sites of DNA damage, we tracked 53BP1-GFP fusion proteins in live-cells upon induction of DSBs with a 405 nm laser (Figure 2A). In control cells 53BP1-GFP was recruited to damaged chromatin within 2

minutes after laser micro-irradiation and was retained at the sites of damage during the 15 minutes of live-cell recording. In contrast, recruitment of 53BP1-GFP to irradiated chromatin was significantly delayed in SETD2-depleted cells (Figure 2A). Importantly, *SETD2* RNAi had no appreciable effects on the total cellular levels of 53BP1-GFP (Figure 2B).

We then investigated whether SETD2 is actively recruited to DSB sites. For that, we engineered a SETD2-GFP fusion protein and tracked it in live cells upon laser-induced DNA damage (Figure 2C and D). In agreement with the lack of fluctuations of the H3K36me3 levels following DSBs (Figure 1A), SETD2-GFP did not accumulate at the laser micro-irradiated regions (Figure 2D).

Since we did not find any evidence for *de novo* histone H3K36 trimethylation during the DDR, we inspected if H3K36me3 is present at the nucleosomes adjacent to the sites of DSBs. In order to have single-nucleosome resolution, U2OS nuclei extracts were digested with micrococcal nuclease (MNase). Analysis of the MNase-digested extracts revealed that the majority of the DNA fragments were approximately 150bp, which is consistent with the length of mono-nucleosomal DNA (Figure 2 – figure supplement 1). Furthermore, each of the four nucleosomal histones was detected in H3K36me3 pull downs, indicating that isolated nucleosomes remained intact (Figure 2E). 53BP1 and H3K36me3 were immunopurified from the mono-nucleosome preparations and the complexes were immunobloted with antibodies against γH2AX and H3K36me3 (Figure 2F). In control (i.e. undamaged) cells, γH2AX was neither detected in the input sample (total cell lysates) nor in any of the two pull-downs (Figure 2F). Upon treatment with NCS a robust signal for γH2AX was observed in the input lane and in the samples immunopurified with antibodies against 53BP1 or H3K36me3, indicating the activation of the DDR (Figure 2F). These data reveal that both 53BP1 and H3K36me3 are present in the same nucleosomes that acquire γH2AX upon DNA damage. Moreover, 53BP1 was detected in complexes immunoprecipitated with the H3K36me3 antibody upon induction of DSBs (Figure 2F). This suggests that H3K36me3 decorates at least a fraction of the nucleosomes to which 53BP1 binds. Altogether, these findings further support the view that H3K36me3 contributes to the establishment of the chromatin state that coordinates the recruitment and activation of DDR factors, even though SETD2 is not actively recruited to DNA damage sites.

SETD2 is required for RAD51 recruitment during homologous recombination repair

The binding of 53BP1 to damaged chromatin tilts the balance between the DNA repair pathways towards NHEJ by preventing 5' end resection of the broken DNA ends (Bouwman et al, 2010; Bunting et al, 2010; Chapman et al, 2012). We therefore investigated whether SETD2 depletion favors DNA 5' end resection and repair of DSBs by HR. To this end we quantified the DNA in the vicinity of a DSB created by the *I-Sce*I nuclease using the DR-GFP reporter assay (Moynahan & Jasin, 2010; Pierce et al, 1999). Upon depletion of *SETD2* by RNAi, the amount of DNA measured by quantitative real-time PCR at 250bp, 300bp, 350bp and 2200bp apart from the *I-Sce*I site was only 53%, 62%, 57% and 71%, respectively, of the DNA levels present in control cells (Figure 3A). These data reveal that ablation of SETD2 leads to persistent DNA 5' end resection of DSBs. In agreement, phosphorylation of RPA (pRPA), an event that is directly linked to efficient DNA 5' end resection (Sartori et al, 2007), was detected in SETD2-depleted cells within the first hour after DNA damage with NCS and reached equilibrium after 6 to 8 hours when its levels were similar to control cells (Figure 3B). Following DNA damage, the recruitment of RPA to DNA repair centers is revealed by the formation of repair-associated foci, a process that can be visualized by immunofluorescence (Figure 3C). At 8 hours after NCS treatment, widespread RPA foci were observed in the nuclei of both control and *SETD2* RNAi cells, suggesting that recruitment of RPA to DNA lesion sites is independent of SETD2 activity. As expected, RPA foci were visible only in cyclin A-positive cells that are in S or G2 phase of the cell cycle (Figure 3C).

The HR–mediated repair of DSBs requires the recruitment of different DNA-repair factors including BRCA1 to the site of damage. BRCA1 cooperates with Mre11–Rad50–Nbs1 (MRN) complex and C-terminal binding protein interacting protein (CtIP) to catalyze 5' to 3' DNA resection of the broken DNA ends (Chapman et al, 2012). Upon NCS treatment, abundant BRCA1 foci were formed in control and SETD2-depleted cells that stained positively for cyclin A (Figure 4A). This result is consistent with the SETD2-independent DNA 5' end resection and suggests that BRCA1 recruitment to DSBs is largely unaffected by SETD2 depletion (Figure 4A).

BRCA1-mediated DNA 5' end resection and phosphorylation of RPA precede the formation of RAD51 filaments on the DNA single-stranded 3' overhangs that promote the search for

homologous DNA sequences and strand exchange (Wyman & Kanaar, 2006). We then inspected the recruitment of RAD51 to broken DNA ends on control and SETD2-depleted cells. RAD51 foci were detected on cells that were in S or G2 phase, as revealed by the positive staining of cyclin A (Figure 4B). Notably, RAD51 was recruited to DSBs in a SETD2-dependent manner. Upon *SETD2* RNAi-depletion, the percentage of U2OS cells with ≥5 foci at 8h and 24h post-NCS treatment (17% and 30%, respectively) was significantly reduced in comparison to control cells (36% and 46%) (Figure 4B). These data establish a presynaptic role of SETD2 that promotes the recruitment of RAD51 to resected DNA ends.

To directly evaluate the impact of this SETD2-dependent role on the efficiency of HR, we depleted SETD2 from U2OS cells stably expressing the DR-GFP reporter. The DR-GFP reporter allows homology-directed repair to be scored by flow cytometry owing to the correction of an inactive *GFP* gene through HR-dependent gene conversion (Figure 5) (Moynahan & Jasin, 2010; Pierce et al, 1999). Ectopic expression of *I-Sce*I in DR-GFP reporter cells led to an average cutting efficiency of the *I-Sce*I restriction site located on the inactive *GFP* gene of 35% (control cells) and 33% (*SETD2* RNAi). In agreement with the impaired RAD51 recruitment, SETD2-depleted cells exhibited a strong reduction (~50%) in HR without detectable differences in the cell cycle progression (Figure 5A and B).

ccRCC cells with *SETD2* inactivating mutations display impaired DDR

A high frequency of *SETD2* mutations was recently disclosed in several cancers, of which clear cell renal cell carcinoma (ccRCC) shows the highest *SETD2* mutation rate (Dalgliesh et al, 2010; Varela et al, 2011). Our present findings suggest that impaired DDR proficiency constitutes a hallmark of *SETD2* mutant cancers and could reveal a novel mechanism through which SETD2 suppresses tumor development and growth. To further test this view, we inspected the DDR in ccRCC cell lines containing inactivating mutations in *SETD2* that result in a strong reduction of H3K36me3 levels (Figure 6A) (Duns et al, 2010). Notably, induction of DSBs in the ccRCC cells resulted in activation of the DDR in a SETD2-dependent manner. Two different *SETD2* wild-type (wt) cell lines (RCC-JW and Caki-2) responded to DNA damage with the rapid formation of γH2AX foci and ATM phosphorylation within the first 30 minutes of the DDR (Figure 6B, C and D). In contrast, DNA repair

was significantly impaired in two *SETD2* mutant ccRCC cell lines (RCC-MF and RCC-FG2) as revealed by the lack of γH2AX foci and ATM phosphorylation upon induction of DSBs (Figure 6B, C and D). These data recapitulate the phenotype of *SETD2* RNAi-depleted U2OS cells and suggest that defects in the DDR are a hallmark of cancer cells with *SETD2* mutations. We then attempted to perform a genetic complementation experiment with our SETD2-GFP transgene to rescue the *SETD2* mutant phenotype. However, despite our efforts, we were not able to obtain a *SETD2* mutant ccRCC cell population expressing the transgene. One possibility is that loss of SETD2 function in the mutant ccRCC cells feeds a cellular proliferation mechanism that if disrupted upon transfection of the wt SETD2-GFP decreases cell viability. Nevertheless, we consistently observed a similar phenotype of impaired DDR in 4 different ccRCC cell lines (RCC-ER; -FG2; -AB; -MF) carrying inactivating mutations in distinct regions of *SETD2* (Duns et al, 2010). Amongst the *SETD2* mutant cell lines RCC-FG2 had the lowest levels of H3K36me3 and showed the strongest impairment in the DDR signaling as revealed by the lack of detectable pATM and γH2AX (Figure 6D). We shall note that RCC-JW cells carry a missense mutation on *SETD2* exon 3, which does not interfere with the methyltransferase activity of the enzyme, and for this reason we classified them as *SETD2* wt (Figure 6C) (Duns et al, 2010). In fact, concerning the DDR, RCC-JW cells behaved equally to two additional *SETD2* wt ccRCC cell lines (Caki-1 and Caki-2) that were also used on our experiments.

To investigate if alternative DDR pathways were able to efficiently repair the DSBs in the *SETD2* mutant cells, we measured the kinetics of DNA repair in ccRCC cells using comet assays (Figure 7). Chemical induction of DSBs yielded a similar degree of DNA damage in both *SETD2* wt and mutant ccRCC cells, as revealed by the comparable fraction of DNA that migrated away from the nuclei and was detected in the comets tails immediately after etoposide treatment (Figure 7). However, these cells differed in their ability to repair the chemically induced DSBs. The amount of fragmented DNA decreased 35% after 3 hours and 45% after 6 hours in the wt cells, which compared to a maximum of 27% reduction observed in mutant cells 6 hours after DNA damage (Figure 7). These results were recapitulated with an additional set of *SETD2* wt and mutant ccRCC cells, which repaired 49% (Caki-2) and 31% (RCC-FG2) of the DNA damage in 6 hours (Figure 7 – figure supplement 1). These findings reveal that the impaired DDR observed in *SETD2* mutant cells

translates into a massive failure to repair DSBs, which is likely to impact severely on genomic stability and may sustain the tumorigenic phenotype.

Inactivation of SETD2 severs the p53-mediated checkpoint despite persistent DNA damage

In circumstances where DNA damage reaches an irreversible stage, specific cell cycle checkpoints are in place to prevent catastrophic cell cycle progression (Kastan & Bartek, 2004; Sperka et al, 2012). The DNA damage checkpoints employ sensor proteins, such as ATM, to detect DNA damage and to initiate signal transduction cascades that activate p53 and inactivate cyclin-dependent kinases causing inhibition of cell cycle progression (Sancar et al, 2004). The tumor suppressor p53 is a direct substrate of ATM kinase (Canman et al, 1998) and is a master effector of the DNA damage cell cycle checkpoints (Sperka et al, 2012). Under normal conditions, p53 protein levels are low owing to MDM2-mediated ubiquitylation and proteasomal degradation. Upon DNA damage, p53-phosphorylation inhibits its interaction with MDM2, resulting in p53 stabilization (Banin et al, 1998; Shieh et al, 1997). We therefore evaluated both p53 phosphorylation and its total protein levels in response to DNA damage. The two *SETD2* wt ccRCC cell lines (RCC-JW and Caki-2) responded to DSBs with p53 phosphorylation and increased total p53 protein levels 2 hours after initiating the DDR (Figure 8A). In contrast, despite the persistent DNA damage caused by the impaired DDR, *SETD2* mutant ccRCC cells (RCC-MF and RCC-FG2) evaded the cell cycle checkpoint as revealed by the low levels of p53 phosphorylation and unnoticeable change of its total protein levels (Figure 8A). Activation of the p53 checkpoint leads to increased gene expression levels of several downstream targets including *CDKN1A*, also known as *p21* (Sperka et al, 2012). Indeed, p21 protein levels rose significantly 2 hours after DNA damage in *SETD2* wt cells, but not in their mutant counterparts (Figure 8A). To exclude the contribution of SETD2-independent mechanisms due to the different genetic backgrounds of the *SETD2* wt and mutant cells, we measured p53 checkpoint activation in *SETD2* RNAi cells upon treatment with etoposide, NCS or phleomycin (Figure 8B, C and D). *SETD2* RNAi-depleted ccRCC cells phenocopied the severed p53 cell cycle checkpoint observed in *SETD2* mutant ccRCC cells. In response to each of the three DNA-damaging agents, control cells increased the total levels of p53 and p21, whereas SETD2-

depleted cells failed to activate p53 (Figure 8B, C and D).

To further examine whether SETD2 is necessary for DNA damage-induced cell-cycle checkpoints, we performed flow cytometry-based cell-cycle profiling analyses in control and *SETD2* RNAi depleted U2OS cells. Cells were treated with phleomycin to activate G1/S and G2/M DNA damage checkpoints. After phleomycin treatment, 49% (8h) and 46% (12h) of control cells were arrested at G1 phase and 34% (8h) and 38% (12h) stayed in G2 phase (Figure 9A). In contrast, only 42% (8h) and 34% (12h) of cells were arrested in G1 phase, whereas 41% (8h) and 48% (12h) were at G2 phase upon SETD2 depletion. These results suggest that SETD2 depletion leads to a defective G1/S cell-cycle arrest, which is in agreement with the deficient activation of p53.

To investigate whether SETD2 affects the cell survival rate in response to DNA damage, we depleted U2OS cells for *SETD2* by RNAi and tested their capacity for clonogenic survival after phleomycin treatment (Figure 9B). Ten days after DNA damage, the colony-forming capacity of control cells was significantly higher than SETD2-depleted cells. This result suggests that SETD2 is a determinant of cell survival after DNA damage.

Combined, these data point to a novel role of SETD2 that can explain the puzzling observation that ccRCC often evade the p53 cell cycle checkpoint despite a very low frequency of *TP53* mutations (Dalgliesh et al, 2010; Gurova et al, 2004; Sato et al, 2013).

Discussion

In this study, by focusing on the pathways that repair DSBs upon RNAi depletion of *SETD2*, we reveal that this histone methyltransferase is necessary for the DDR. We show that SETD2 is required for the activation of ATM following DNA damage. In agreement with the impaired ATM activation, spreading of γH2AX and 53BP1 phosphorylation were greatly compromised in SETD2-depleted cells treated with NCS or etoposide, but only marginally affected in DSBs induced by phleomycin. These findings suggest that the DNA damage signaling may follow multiple pathways with different requirements for H3K36me3 and can result in phosphorylation of H2AX and 53BP1 independently of ATM activation. In fact, ionizing radiation-induced H2AX phosphorylation and recruitment of 53BP1 to DSBs can be carried out by ATM and DNA-dependent protein kinase (DNA-PK) in a redundant manner (Stiff et al, 2004). Moreover, ataxia telangiectasia and Rad3-related protein (ATR) can also phosphorylate many of the ATM substrates, including H2AX (Ward et al, 2001).

53BP1 nucleation at DNA damaged chromatin plays an important role in favoring DNA repair by NHEJ (Bouwman et al, 2010; Bunting et al, 2010; Chapman et al, 2012). In agreement, we found that induction of DSBs resulted in a significant impairment of the 53BP1 recruitment and increased DNA 5' end resection in SETD2-depleted cells. However, the increased resection did not reflect increased efficiency of HR repair. Instead, persistent DNA 5' end resection is likely due to the roadblock in the HR pathway that is created by the failure of RAD51 binding to the single-stranded DNA. Indeed, this defect in presynaptic filament formation on the resected DNA resulted in a 50% reduction in the efficiency of gene conversion of the DR-GFP HR reporter. Exonuclease-mediated resection of DNA ends is known to promote phosphorylation of RPA and to orchestrate an ATM-to-ATR switch at DNA breaks (Shiotani & Zou, 2009). This switch in the main DNA damage sensor provides a reasonable explanation for the RPA phosphorylation and the proficient RPA recruitment to DSBs despite the impaired ATM activation in SETD2-depleted cells. Alternatively, ATM-independent RPA phosphorylation can also be achieved through the activity of DNA-PK (Anantha et

al, 2007; Shao et al, 1999).

Lens epithelium–derived growth factor p75 splice variant (LEDGF) is a H3K36me3-binding protein that promotes the HR repair of DSBs (Daugaard et al, 2012). Depletion of LEDGF impairs the recruitment of CtIP and the subsequent DNA 5' end resection of DSBs. While defects in LEDGF recruitment to DSBs may account for the impaired HR phenotype that we report in SETD2 deficient cells, our data supports an extended LEDGF-independent role of SETD2 in the repair of DSBs by HR. Our findings that DNA 5' end resection and RPA foci formation are not severely compromised in SETD2-depleted cells disclose a specific presynaptic role for SETD2 that is necessary for the recruitment of RAD51 to single-stranded DNA. One possibility is that H3K36me3 defines a local chromatin state that favors the recruitment of RAD51 to DSBs and successful HR repair. This could be achieved by the FACT histone chaperone upon recruitment to H3K36me3 marked nucleosomes (Carvalho et al, 2013). In agreement with this view, depletion of the FACT subunit SPT16 results in a major impairment of HR (Kari et al, 2011; Oliveira et al, 2014). FACT is required to recruit the ubiquitin ligase RNF20, which in turn facilitates RAD51 accumulation at DSBs (Oliveira et al, 2014). The view that changes in chromatin dynamics may affect RAD51 function is not completely unexpected as illustrated by the role of the histone acetyltransferase 1 (HAT1) in RAD51 during HR (Yang et al, 2013). HAT1 promotes acetylation of histone H4 as well as incorporation of histone variant H3.3 at DSBs and facilitates RAD51 recruitment and efficient HR repair. Nevertheless, the major impact of SETD2 on RNA polymerase II transcription and pre-mRNA processing that others and we have previously described (reviewed in de Almeida & Carmo-Fonseca, 2014) discloses the alternative possibility that the impaired formation of RAD51 filaments and HR may result from disrupted gene expression of key DNA repair factors. Hence, additional studies are needed to fully elucidate the mechanistic basis of the SETD2 impact on the DDR.

Unlike all histone modifications found to promote the DDR, previous studies (Pei et al, 2011) and our data show no evidence of increased H3K36me3 levels at the DNA damage sites or of a DDR-dependent recruitment of SETD2 to DSBs. These findings disclose an unprecedented role for a histone-modifying enzyme in priming intact chromatin for the response to DNA damage. A model that emphasizes the regulation of the H3K36me3 accessibility as a major determinant of the DDR can be envisaged. According to this view, the conformational changes that occur after a DSB may

cause exposure of H3K36me3 marks previously written by SETD2 in intact chromatin, for instance during transcription by RNA polymerase II or replication. In fact, a careful inspection of the nucleosome structure reveals that lysine 36 on the N-terminal tail of histone H3 does not protrude from the nucleosome core. Instead, this lysine is hidden by the DNA double strand that wraps the histone octameric core (Luger et al, 1997). This sheltered location was first described 3 decades ago, when Crane-Robinson and colleagues investigated the accessibility of the histone terminal domains to proteases. Their experiments revealed that while the first 26 N-terminal residues of histone H3 were greatly sensitive to trypsin digestion, H3K36 was resistant to the enzyme (Bohm et al, 1981). According to this “break & access model” DNA damage exposes H3K36me3, which then contributes together with a set of well-defined histone modifications to the orchestration of the chromatin landscape that drives the initial recruitment and activation of DDR factors, such as ATM.

The role of H3K36me3 in promoting repair of DSBs by HR may be particularly relevant at coding regions where the introduction of genomic aberrations is likely to have deleterious consequences. Therefore, in these regions the choice between error-prone NHEJ and the more reliable HR pathway is of utmost importance. In fact, most H3K36me3 is found at actively transcribed chromatin where it signals the recruitment of the histone chaperone FACT to reassemble nucleosomes in the wake of RNA polymerase II elongation (Carvalho et al, 2013). Should a DSB amputate a coding region, exposure of H3K36me3 previously deposited by SETD2 travelling with the transcriptional machinery may promote DNA repair by HR and would guarantee the integrity of the genetic information.

From all cancers on which *SETD2* mutations have been reported, ccRCC shows the highest mutation rate (Dalgliesh et al, 2010; Varela et al, 2011). Our present findings reveal that *SETD2* mutant ccRCC cells have impaired DDR signaling which leads to inefficient repair of DNA damage. However, the p53-dependent cell cycle checkpoint is not activated in SETD2-deficient cells despite the persistence of DNA damage. Depletion of SETD2 abrogates p53 activation, and leads to eviction of the G1/S checkpoint upon DNA damage. In addition to the defects in the DNA damage signaling that we found in SETD2-depleted cells, which could extend to improper p53 activation, it is also possible that SETD2 impinges directly on p53 activity and activation of its downstream targets through direct protein-protein interactions (Xie et al, 2008). Furthermore, in the absence of SETD2,

the capacity for clonogenic survival following DNA damage is significantly reduced. These findings integrate SETD2 into the p53 regulatory network and provide a reasonable explanation for the intriguing observation that inactivation of this master regulator of cell cycle checkpoints in ccRCC is rarely caused by mutations in *TP53* (Dalgliesh et al, 2010; Gurova et al, 2004; Sato et al, 2013).

A plethora of recent studies has revealed that mutation rates and genomic instabilities in cancer are directly related to aberrant histone modifications and chromatin organization, underscoring the importance of the histone code in maintaining genome stability (Lukas et al, 2011; Papamichos-Chronakis & Peterson, 2013). CcRCC is an example of a cancer where a high rate of genomic alterations occurs in parallel to inactivating mutations and deletions of histone modifiers, such as *SETD2* (Cancer Genome Atlas Research, 2013; Sato et al, 2013). The present study provides a functional link between these two events extending our understanding of the impact of altered chromatin states on the mechanisms that maintain genome integrity. Although it is now evident that alterations in histone modifications are a hallmark of most cancers, it is still unclear whether these changes are drivers or passengers of tumorigenesis (Waldmann & Schneider, 2013). Our findings endorse the classification of SETD2 as a tumor suppressor and place inactivating mutations in this histone modifier at the peak of a harmful cascade of events that may ultimately drive malignant cell transformation and tumor development.

Materials and Methods

Cell culture and drug treatments

Human osteosarcoma (U2OS) cells (ATCC) and the ccRCC cells RCC-JW, Caki-2, RCC-MF and RCC-FG2 (Duns et al, 2010) (Cell Line Services Eppelheim, Germany) were grown as monolayers in Dulbecco's modified Eagle medium – DMEM (Invitrogen), supplemented with 10% (v/v) FBS, 1% (v/v) nonessential amino acids, 1% (v/v) L-glutamine and 100U/ml penicillin-streptomycin, and maintained at 37°C in a humidified atmosphere containing 5% CO_2. To induce DNA damage, cells were treated with 50μM etoposide (Sigma) for 15min, 250ng/ml neocarzinostatin (NCS) (Sigma) for 30min or 40μM phleomycin (Sigma) for 30 min, washed and harvested immediately after the treatment and at the indicated time-points.

RNA interference

SETD2 RNAi was achieved using three different synthetic siRNA duplexes targeting *SETD2* (Eurogentec) (Carvalho et al, 2013). In each experiment, at least two different siRNAs were used resulting in similar knockdown efficiencies. siRNAs targeting the firefly luciferase (GL2) were used as controls (Eurogentec) (Elbashir et al, 2001). Cells were reverse transfected with 10μM siRNAs using OptiMEM (Invitrogen) and Lipofectamine RNAiMAX (Invitrogen), according to the manufacturer's instructions. 24 hours after the first transfection, cells were re-transfected with the same siRNA duplexes and transfection reagents and harvested on the following day.

SETD2-GFP plasmid construction

The *SETD2* cDNA was cloned into the pEGFP-C1 vector (Clontech) in a ligation reaction containing two fragments. A fragment containing 5257bp from the 3' end of *SETD2* was obtained by digestion of pCR-XL-TOPO-SETD2 (Thermo Scientific, clone 40125713) with *Spe*I and *Pst*I. A fragment containing the 5' end of *SETD2* was obtained by PCR amplification of pCR-XL-TOPO-SETD2 using

primers containing *Bgl*II and *Spe*I restriction sites. The PCR product was digested with *Bgl*II and *Spe*I restriction enzymes and purified. Both fragments were co-inserted in *Bgl*II/*Pst*I digested pEGFP-C1 vector. This construct was confirmed by DNA sequencing.

Immunofluorescence

U2OS cells grown on coverslips were fixed with 3.7% paraformaldehyde for 10min at room temperature. Cells were then permeabilized with 0.5% Triton X-100/PBS for 10min. Incubation with primary antibodies against γH2AX (phosphoSer139; 05-636, Millipore), total RPA32 (ab2175, Abcam), BRCA1 (sc-6954, Santa Cruz Biotechnology), RAD51 (ab213, Abcam) or cyclin A (sc-751, Santa Cruz Biotechnology) was followed by incubation with fluorochrome-conjugated (Alexa Fluor 488 and 594) antibodies (Jackson Immunoresearch). All the washing steps were done with PBS containing 0.05% (v/v) Tween 20. The samples were mounted in Vectashield (H-1000, Vector Laboratories) with 4'-6-diamidino-2-phenylindole (Dapi) (09542, Sigma) to stain the DNA. A Zeiss LSM 710 (Carl Zeiss) confocal microscope was used to visualize the cells with a 63x/1.4 oil immersion or a 40x objective.

Western blot

Whole cell protein extracts were prepared by cell lysis with SDS-PAGE buffer (80mM Tris-HCL pH 6.8, 16% glicerol, 4.5% SDS, 450mM DTT, 0.01% bromophenol blue) with 200U/ml benzonase (Sigma) and 50 μM $MgCl_2$ and boiling for 5min. Equal amounts of protein extracts were resolved by SDS-polyacrylamide gel electrophoresis (SDS-PAGE) and transferred to a nitrocellulose membrane. Immunobloting was performed with antibodies against the following proteins: H3K36me3 (ab9050, Abcam), histone H3 (ab1791, Abcam), phospho-53BP1 (phosphoSer1778; No.2675, Cell Signaling), phospho-ATM (phosphoS1981; No.200-301-400s, Rockland), total ATM (PC116, Millipore), total RPA32 (ab2175, Abcam), phospho-RPA32 (phosphoSer4/Ser8; A300-245A, Bethyl), α-Tubulin (T5168, Sigma); γH2AX (phosphoSer139; 05-636, Millipore); Histone H2B (ab1790, Abcam); GFP (11814460001, Roche); total p53 (sc-263, Santa Cruz); phospho-p53 (phosphoSer15; ab38497, Abcam); p21 (sc-397, Santa Cruz).

Laser induced DNA damage

Laser-induced DSBs were generated using a confocal microscope (LSM 510 Meta, Carl Zeiss) equipped with a 37ºC heating chamber (Pecon) and a 405nm diode laser focused through a 63x/1.4 oil immersion objective. We performed one iteration at a laser output of 100%. To follow the dynamics of GFP-tagged 53BP1 (53BP1-GFP, a kind gift from Dr Jiri Lukas, Danish Cancer Society, Copenhagen, Denmark) or SETD2-GFP during the DDR, live-cell images were recorded during 15min after laser-irradiation. Control or SETD2-depleted U2OS cells were transfected with expression plasmids for 53BP1-GFP or SETD2-GFP using Lipofectamine 2000 (Invitrogen) according to the manufacturers' protocol.

Nuclear Co-immunoprecipitation

Briefly, nuclear extracts and further MNase digestion was performed as described earlier (Carvalho et al, 2013) with minor changes. Cells were lysed in ice-cold NP-40 buffer (10 mM Tris-HCl (pH 7.4), 10 mM NaCl, 3mM MgCl2, 0.5% Nonidet P-40, 0.15 mM spermine and 0.5 mM spermidine) and isolated nuclei were washed and resuspended in MNase digestion buffer (10 mM Tris-HCl (pH 7.4), 15 mM NaCl, 60 mM KCl, 0.15 mM spermine and 0.5 mM spermidine) and sonicated with a single pulse of 15 seconds at 50% intensity using a Soniprep 150 (Sanyo). Nuclei were digested enzymatically with 60U MNase (Thermo Scientific) at 4ºC for 60minutes. MNase stop buffer (100 mM EDTA and 10 mM EGTA (pH 7.5)) was used to stop the reaction and samples were pre-cleared using Protein G Dynabeads (Life technologies) at 4ºC for 45minutes. All buffers were supplemented with protease and phosphatase inhibitors (Roche). Samples were incubated with 3µg of either anti-53BP1 (ab87097, Abcam) or anti-H3K36me3 (ab9050, Abcam) antibodies overnight at 4ºC. The protein complexes were pulled down using Protein G Dynabeads, washed six times in IP buffer (200mM NaCl, 16.7mM Tris pH 8.1, 1.1% TritonX-100, 1.2mM EDTA, 0.01% SDS) and resolved by SDS-PAGE before immunobloting with antibodies against: γH2AX (phosphoSer139; 05-636, Milipore) and anti-H3K36me3 (ab9050, Abcam). $1/10^{th}$ of the total cell lysate was used as input samples.

Homologous recombination reporter assay

The U2OS DR-GFP cells were a kind gift of Dr Maria Jasin from the Memorial Sloan-Kettering, USA. To assess HR efficiency, U2OS DR-GFP cells were seeded in a 6 well plate and reverse transfected with the *I-Sce*I expression plasmid (pCBA-SceI, 26477 Addgene) using Lipofectamine 2000 (Invitrogen), according to the manufacturers' protocol. Cells were maintained for 24h at 37°C in a humidified atmosphere containing 5% CO_2. After 24h, siRNAs targeting either firefly luciferase (GL2) or *SETD2* were transfected using Lipofectamine RNAiMAX (Invitrogen). 48h after RNAi (and 72h after *I-Sce*I transfection) cells were harvested and subjected to flow cytometry analysis (FACS Calibur, BD Biosciences) with a minimum of 20000 events acquired. The enzyme cutting efficiency (35% on control cells and 33% on SETD2-depleted cells) was determined by real-time quantitative PCR (RT-qPCR) with primers flanking the *I-Sce*I cleavage site on the *GFP* reporter gene. The amount of DNA was estimated as follows: 2^(Ct reference – Ct sample), where Ct reference and Ct sample are mean threshold cycles of RT-qPCR done in duplicate from *GAPDH* (reference) and the DNA flanking the *I-Sce*I site (sample). Non-transfected cells were used as a reference to calculate the percentage of cutting upon *I-Sce*I transfection. Primers are detailed in Table 1. The percentage of GFP+ cells was estimated using FlowJo (TreeStar).

Cell cycle analysis and survival assays

The nuclear DNA content was estimated by flow cytometry analysis of cells stained with propidium iodide (PI). Briefly, cultured cells were collected by trypsinization and fixed by drop wise addition of ice-cold 50% ethanol with gentle vortexing. After placing the samples 24h on ice, RNase was added to a final concentration of 50µg/ml and incubated for 30min at 37°C. Following addition of PI (100µg/ml), 80000 events were acquired on a FACS Calibur (BD Biosciences) and the DNA content analyzed with FlowJo (TreeStar). For analysis of cell cycle checkpoints, control or SETD2-depleted U2OS cells were treated with 40µM phleomycin for 30 minutes, washed and cultured in fresh medium for 8 and 12 hours before flow cytometry analysis of the cell cycle progression. For analysis of clonogenic survival, cells were reverse-transfected with SETD2 and control (GL2) siRNAs, seeded in 10 cm dishes (1,000 cells/dish) and 2 days later treated for 30min with phleomycin at various concentrations. Cells were then cultured for 10 days and individual colonies counted upon staining with crystal violet.

Direct measurement of DNA 5' end resection

The extent of DNA 5' end resection was analyzed by RT-qPCR analysis of the DNA surrounding the *I-Sce*I site of the *GFP* gene integrated in the U2OS cells (U2OS DR-GFP reporter) transfected with the *I-Sce*I expression plasmid. Primers flanking the *I-Sce*I site and four regions located approximately 250bp, 300bp, 350bp and 2200bp away from this site were used. The housekeeping gene *GAPDH* was used as a genomic DNA control. RT-qPCR was performed in the ViiA Real Time PCR (Applied Biosystems) using Power SYBR® Green PCR Master Mix (Applied Biosystems). The percentage of digestion was estimated as follows: 2^(Ct reference – Ct sample), where Ct reference and Ct sample are mean threshold cycles of RT-qPCR done in duplicate on DNA samples from *GAPDH* (reference) and the DNA regions surrounding the *I-Sce*I site (sample). The amount of DNA was corrected for the *I-Sce*I digestion efficiency by normalizing the data against the amount of DNA flanking the restriction site. All primer sequences are presented in Table 1.

Comet assays

DNA double-strand breaks in *SETD2* wt or mutant ccRCC cells were detected by neutral comet assay using the CometAssay kit (Trevigen) according to the manufacturer's instructions. A Zeiss Axiovert 200M (Carl Zeiss) microscope equipped with a 20x objective was used to visualize cells. The amount of DNA damage was estimated by measuring the percentage of fluorescence in the comet's tail using the CometScore analysis software.

Statistical analysis

Where indicated, data were subjected to a two-tailed Student's t-test to resolve statistical significance.

Acknowledgements

We thank our colleagues Dr Maria Carmo-Fonseca and Dr Miguel Godinho-Ferreira for critical comments and suggestions. We thank Ana Rita Grosso, Ana Luísa Caetano, Mafalda Matos, Sérgio Marinho and Pedro Pereira for technical assistance. We are grateful to Dr Maria Jasin and Dr Jiri Lukas for kindly providing the U2OS DR-GFP cells and 53BP1-GFP expression plasmid, respectively. We also thank the Bioimaging and Flow Cytometry facilities of the IMM for technical assistance. This work was supported by grants from Fundação para a Ciência e Tecnologia (FCT), Portugal (PTDC-BIA-BCM-111451-2009 and PTDC/BIM-ONC/0384-2012 to SFdA). ACV is a Lisbon BioMed PhD fellow funded by FCT (SFRH/BD/52232/2013). SCS is supported by RNPnet, a Marie Curie Initial Training Network (PITN-GA-2011-289007). JF receives support from a Gulbenkian Foundation grant (96526/2009). SFdeA is the recipient of a FCT Investigator award.

Author Contributions

SC, ACV and SFdA conceived the project and designed the experiments. SC, ACV, SCS, FBM, ACR, JMPD, JF and SFdA performed experiments. SC, ACV, FBM, JMPD, JF and SFdA analyzed and discussed the data. SFdA wrote the manuscript with the assistance of SC and ACV. All authors reviewed the manuscript.

Competing interests

The authors declare that they have no competing interests in relation to the submitted work.

References

Anantha RW, Vassin VM, Borowiec JA (2007) Sequential and synergistic modification of human RPA stimulates chromosomal DNA repair. *J Biol Chem* **282:** 35910-35923

Banin S, Moyal L, Shieh S, Taya Y, Anderson CW, Chessa L, Smorodinsky NI, Prives C, Reiss Y, Shiloh Y, Ziv Y (1998) Enhanced phosphorylation of p53 by ATM in response to DNA damage. *Science* **281:** 1674-1677

Bohm L, Briand G, Sautiere P, Crane-Robinson C (1981) Proteolytic digestion studies of chromatin core-histone structure. Identification of the limit peptides of histones H3 and H4. *European journal of biochemistry / FEBS* **119:** 67-74

Bouwman P, Aly A, Escandell JM, Pieterse M, Bartkova J, van der Gulden H, Hiddingh S, Thanasoula M, Kulkarni A, Yang Q, Haffty BG, Tommiska J, Blomqvist C, Drapkin R, Adams DJ, Nevanlinna H, Bartek J, Tarsounas M, Ganesan S, Jonkers J (2010) 53BP1 loss rescues BRCA1 deficiency and is associated with triple-negative and BRCA-mutated breast cancers. *Nat Struct Mol Biol* **17:** 688-695

Bunting SF, Callen E, Wong N, Chen HT, Polato F, Gunn A, Bothmer A, Feldhahn N, Fernandez-Capetillo O, Cao L, Xu X, Deng CX, Finkel T, Nussenzweig M, Stark JM, Nussenzweig A (2010) 53BP1 inhibits homologous recombination in Brca1-deficient cells by blocking resection of DNA breaks. *Cell* **141:** 243-254

Burden DA, Kingma PS, Froelich-Ammon SJ, Bjornsti MA, Patchan MW, Thompson RB, Osheroff N (1996) Topoisomerase II.etoposide interactions direct the formation of drug-induced enzyme-DNA cleavage complexes. *J Biol Chem* **271:** 29238-29244

Cancer Genome Atlas Research N (2013) Comprehensive molecular characterization of clear cell renal cell carcinoma. *Nature* **499:** 43-49

Canman CE, Lim DS, Cimprich KA, Taya Y, Tamai K, Sakaguchi K, Appella E, Kastan MB, Siliciano JD (1998) Activation of the ATM kinase by ionizing radiation and phosphorylation of p53. *Science* **281:** 1677-1679

Carvalho S, Raposo AC, Martins FB, Grosso AR, Sridhara SC, Rino J, Carmo-Fonseca M, de Almeida SF (2013) Histone methyltransferase SETD2 coordinates FACT recruitment with nucleosome dynamics during transcription. *Nucleic Acids Res* **41:** 2881-2893

Chapman JR, Taylor MR, Boulton SJ (2012) Playing the end game: DNA double-strand break repair pathway choice. *Mol Cell* **47:** 497-510

Dalgliesh GL, Furge K, Greenman C, Chen L, Bignell G, Butler A, Davies H, Edkins S, Hardy C, Latimer C, Teague J, Andrews J, Barthorpe S, Beare D, Buck G, Campbell PJ, Forbes S, Jia M, Jones D, Knott H, Kok CY, Lau KW, Leroy C, Lin ML, McBride DJ, Maddison M, Maguire S, McLay K, Menzies A, Mironenko T, Mulderrig L, Mudie L, O'Meara S, Pleasance E, Rajasingham A, Shepherd R, Smith R, Stebbings L, Stephens P, Tang G, Tarpey PS, Turrell K, Dykema KJ, Khoo SK, Petillo D, Wondergem B, Anema J, Kahnoski RJ, Teh BT, Stratton MR, Futreal PA (2010) Systematic sequencing of renal carcinoma reveals inactivation of histone modifying genes. *Nature* **463:** 360-363

598 Daugaard M, Baude A, Fugger K, Povlsen LK, Beck H, Sørensen CS, Petersen NH, Sorensen PH,
599 Lukas C, Bartek J, Lukas J, Rohde M, Jäättelä M (2012) LEDGF (p75) promotes DNA-end resection
600 and homologous recombination. *Nat Struct Mol Biol* **19**:803-10
601
602 de Almeida SF, Carmo-Fonseca M (2014) Reciprocal regulatory links between cotranscriptional
603 splicing and chromatin. *Semin Cell Dev Biol* pii: S1084-9521(14)00038-X. doi:
604 10.1016/j.semcdb.2014.03.010. epub ahead of print
605
606 de Almeida SF, Garcia-Sacristan A, Custodio N, Carmo-Fonseca M (2010) A link between nuclear
607 RNA surveillance, the human exosome and RNA polymerase II transcriptional termination. *Nucleic*
608 *acids research* **38:** 8015-8026
609
610 Duns G, van den Berg E, van Duivenbode I, Osinga J, Hollema H, Hofstra RM, Kok K (2010)
611 Histone methyltransferase gene SETD2 is a novel tumor suppressor gene in clear cell renal cell
612 carcinoma. *Cancer Res* **70:** 4287-4291
613
614 Edmunds JW, Mahadevan LC, Clayton AL (2008) Dynamic histone H3 methylation during gene
615 induction: HYPB/Setd2 mediates all H3K36 trimethylation. *EMBO J* **27:** 406-420
616
617 Elbashir SM, Harborth J, Lendeckel W, Yalcin A, Weber K, Tuschl T (2001) Duplexes of 21-
618 nucleotide RNAs mediate RNA interference in cultured mammalian cells. *Nature* **411:** 494-498
619
620 Fontebasso AM, Schwartzentruber J, Khuong-Quang DA, Liu XY, Sturm D, Korshunov A, Jones DT,
621 Witt H, Kool M, Albrecht S, Fleming A, Hadjadj D, Busche S, Lepage P, Montpetit A, Staffa A,
622 Gerges N, Zakrzewska M, Zakrzewski K, Liberski PP, Hauser P, Garami M, Klekner A, Bognar L,
623 Zadeh G, Faury D, Pfister SM, Jabado N, Majewski J (2013) Mutations in SETD2 and genes
624 affecting histone H3K36 methylation target hemispheric high-grade gliomas. *Acta neuropathologica*
625 **125:** 659-669
626
627 Goldberg IH (1987) Free radical mechanisms in neocarzinostatin-induced DNA damage. *Free*
628 *radical biology & medicine* **3:** 41-54
629
630 Greenberg RA (2011) Histone tails: Directing the chromatin response to DNA damage. *FEBS Lett*
631 **585:** 2883-2890
632
633 Gurova KV, Hill JE, Razorenova OV, Chumakov PM, Gudkov AV (2004) p53 pathway in renal cell
634 carcinoma is repressed by a dominant mechanism. *Cancer Res* **64:** 1951-1958
635
636 Harper JW, Elledge SJ (2007) The DNA damage response: ten years after. *Mol Cell* **28:** 739-745
637
638 Joseph CG, Hwang H, Jiao Y, Wood LD, Kinde I, Wu J, Mandahl N, Luo J, Hruban RH, Diaz LA, Jr.,
639 He TC, Vogelstein B, Kinzler KW, Mertens F, Papadopoulos N (2014) Exomic analysis of myxoid
640 liposarcomas, synovial sarcomas, and osteosarcomas. *Genes, chromosomes & cancer* **53:** 15-24
641
642 Kari V, Shchebet A, Neumann H, Johnsen SA (2011) The H2B ubiquitin ligase RNF40 cooperates
643 with SUPT16H to induce dynamic changes in chromatin structure during DNA double-strand break
644 repair. *Cell Cycle* **10**:3495-504
645
646 Kastan MB, Bartek J (2004) Cell-cycle checkpoints and cancer. *Nature* **432:** 316-323
647
648 Li F, Mao G, Tong D, Huang J, Gu L, Yang W, Li GM (2013) The histone mark H3K36me3 regulates
649 human DNA mismatch repair through its interaction with MutSalpha. *Cell* **153:** 590-600
650
651 Lieber MR (2010) The mechanism of double-strand DNA break repair by the nonhomologous DNA
652 end-joining pathway. *Annu Rev Biochem* **79:** 181-211
653
654 Luger K, Mader AW, Richmond RK, Sargent DF, Richmond TJ (1997) Crystal structure of the
655 nucleosome core particle at 2.8 A resolution. *Nature* **389:** 251-260

Lukas J, Lukas C, Bartek J (2011) More than just a focus: The chromatin response to DNA damage and its role in genome integrity maintenance. *Nat Cell Biol* **13:** 1161-1169

Matsuoka S, Ballif BA, Smogorzewska A, McDonald ER, 3rd, Hurov KE, Luo J, Bakalarski CE, Zhao Z, Solimini N, Lerenthal Y, Shiloh Y, Gygi SP, Elledge SJ (2007) ATM and ATR substrate analysis reveals extensive protein networks responsive to DNA damage. *Science* **316:** 1160-1166

Moore, CW (1988) Internucleosomal cleavage and chromosomal degradation by bleomycin and phleomycin in yeast. *Cancer Res* **23**: 6837–6843

Moynahan ME, Jasin M (2010) Mitotic homologous recombination maintains genomic stability and suppresses tumorigenesis. *Nat Rev Mol Cell Biol* **11:** 196-207

Oliveira DV, Kato A, Nakamura K, Ikura T, Okada M, Kobayashi J, Yanagihara H, Saito Y, Tauchi H, Komatsu K (2014) Histone chaperone FACT regulates homologous recombination by chromatin remodeling through interaction with RNF20. *J Cell Sci* **127**(Pt 4):763-72

Papamichos-Chronakis M, Peterson CL (2013) Chromatin and the genome integrity network. *Nat Rev Genet* **14:** 62-75

Pei H, Zhang L, Luo K, Qin Y, Chesi M, Fei F, Bergsagel PL, Wang L, You Z, Lou Z (2011) MMSET regulates histone H4K20 methylation and 53BP1 accumulation at DNA damage sites. *Nature* **470:** 124-128

Pierce AJ, Johnson RD, Thompson LH, Jasin M (1999) XRCC3 promotes homology-directed repair of DNA damage in mammalian cells. *Genes Dev* **13:** 2633-2638

Rogakou EP, Pilch DR, Orr AH, Ivanova VS, Bonner WM (1998) DNA double-stranded breaks induce histone H2AX phosphorylation on serine 139. *J Biol Chem* **273:** 5858-5868

San Filippo J, Sung P, Klein H (2008) Mechanism of eukaryotic homologous recombination. *Annu Rev Biochem* **77:** 229-257

Sancar A, Lindsey-Boltz LA, Unsal-Kacmaz K, Linn S (2004) Molecular mechanisms of mammalian DNA repair and the DNA damage checkpoints. *Annu Rev Biochem* **73:** 39-85

Sartori AA, Lukas C, Coates J, Mistrik M, Fu S, Bartek J, Baer R, Lukas J, Jackson SP (2007) Human CtIP promotes DNA end resection. *Nature* **450:** 509-514

Sato Y, Yoshizato T, Shiraishi Y, Maekawa S, Okuno Y, Kamura T, Shimamura T, Sato-Otsubo A, Nagae G, Suzuki H, Nagata Y, Yoshida K, Kon A, Suzuki Y, Chiba K, Tanaka H, Niida A, Fujimoto A, Tsunoda T, Morikawa T, Maeda D, Kume H, Sugano S, Fukayama M, Aburatani H, Sanada M, Miyano S, Homma Y, Ogawa S (2013) Integrated molecular analysis of clear-cell renal cell carcinoma. *Nat Genet* **45:** 860-867

Shao RG, Cao CX, Zhang H, Kohn KW, Wold MS, Pommier Y (1999) Replication-mediated DNA damage by camptothecin induces phosphorylation of RPA by DNA-dependent protein kinase and dissociates RPA:DNA-PK complexes. *EMBO J* **18:** 1397-1406

Shieh SY, Ikeda M, Taya Y, Prives C (1997) DNA damage-induced phosphorylation of p53 alleviates inhibition by MDM2. *Cell* **91:** 325-334

Shiotani B, Zou L (2009) Single-stranded DNA orchestrates an ATM-to-ATR switch at DNA breaks. *Mol Cell* **33:** 547-558

Soria G, Polo SE, Almouzni G (2012) Prime, repair, restore: the active role of chromatin in the DNA damage response. *Mol Cell* **46:** 722-734

Sperka T, Wang J, Rudolph KL (2012) DNA damage checkpoints in stem cells, ageing and cancer. *Nat Rev Mol Cell Biol* **13:** 579-590

Stiff T, O'Driscoll M, Rief N, Iwabuchi K, Löbrich M, Jeggo PA (2004) ATM and DNA-PK function redundantly to phosphorylate H2AX after exposure to ionizing radiation. *Cancer Res* **64**: 2390-6

Varela I, Tarpey P, Raine K, Huang D, Ong CK, Stephens P, Davies H, Jones D, Lin ML, Teague J, Bignell G, Butler A, Cho J, Dalgliesh GL, Galappaththige D, Greenman C, Hardy C, Jia M, Latimer C, Lau KW, Marshall J, McLaren S, Menzies A, Mudie L, Stebbings L, Largaespada DA, Wessels LF, Richard S, Kahnoski RJ, Anema J, Tuveson DA, Perez-Mancera PA, Mustonen V, Fischer A, Adams DJ, Rust A, Chan-on W, Subimerb C, Dykema K, Furge K, Campbell PJ, Teh BT, Stratton MR, Futreal PA (2011) Exome sequencing identifies frequent mutation of the SWI/SNF complex gene PBRM1 in renal carcinoma. *Nature* **469:** 539-542

Waldmann T, Schneider R (2013) Targeting histone modifications--epigenetics in cancer. *Curr Opin Cell Biol* **25:** 184-189

Ward IM, Chen J (2001) Histone H2AX is phosphorylated in an ATR-dependent manner in response to replicational stress. *J Biol Chem* **276**:47759-62

Wyman C, Kanaar R (2006) DNA double-strand break repair: all's well that ends well. *Annu Rev Genet* **40:** 363-383

Xie P, Tian C, An L, Nie J, Lu K, Xing G, Zhang L, He F (2008) Histone methyltransferase protein SETD2 interacts with p53 and selectively regulates its downstream genes. *Cell Signal* **20**:1671-8

Yang X, Li L, Liang J, Shi L, Yang J, Yi X, Zhang D, Han X, Yu N, Shang Y (2013) Histone Acetyltransferase 1 Promotes Homologous Recombination in DNA Repair by Facilitating Histone Turnover. *J Biol Chem* **288**:18271-82

Zhang J, Ding L, Holmfeldt L, Wu G, Heatley SL, Payne-Turner D, Easton J, Chen X, Wang J, Rusch M, Lu C, Chen SC, Wei L, Collins-Underwood JR, Ma J, Roberts KG, Pounds SB, Ulyanov A, Becksfort J, Gupta P, Huether R, Kriwacki RW, Parker M, McGoldrick DJ, Zhao D, Alford D, Espy S, Bobba KC, Song G, Pei D, Cheng C, Roberts S, Barbato MI, Campana D, Coustan-Smith E, Shurtleff SA, Raimondi SC, Kleppe M, Cools J, Shimano KA, Hermiston ML, Doulatov S, Eppert K, Laurenti E, Notta F, Dick JE, Basso G, Hunger SP, Loh ML, Devidas M, Wood B, Winter S, Dunsmore KP, Fulton RS, Fulton LL, Hong X, Harris CC, Dooling DJ, Ochoa K, Johnson KJ, Obenauer JC, Evans WE, Pui CH, Naeve CW, Ley TJ, Mardis ER, Wilson RK, Downing JR, Mullighan CG (2012) The genetic basis of early T-cell precursor acute lymphoblastic leukaemia. *Nature* **481:** 157-163

Figures Legends

Figure 1. SETD2 is necessary for ATM activation during the DNA damage response
Control and *SETD2* RNAi-depleted U2OS cells were challenged with etoposide **(A)**, NCS **(B)** or phleomycin **(C)** and chased in fresh media during the indicated time points. Western blot analysis was performed with antibodies against the indicated proteins. Molecular weight markers (KDa) are shown on the left of each blot. Data are from one representative experiment of at least three independent experiments performed with similar results.

Figure 2. SETD2 promotes 53BP1 recruitment to DNA damage sites
(A) 53BP1-GFP transfected U2OS cells were damaged by laser irradiation of the indicated nuclear region. The dynamics of 53BP1-GFP during the DNA damage response on control and SETD2-depleted cells was monitored by live cell imaging for 15min after laser irradiation. One representative experiment from over 50 individual cells recorded is shown. **(B)** Control and *SETD2* RNAi depleted U2OS cells were transfected with a 53BP1-GFP expression plasmid. Western blot analysis was performed with antibodies against GFP (to detect 53BP1-GFP), H3K36me3, total histone H3 and α-tubulin. Molecular weight markers (KDa) are shown on the left. **(C)** SETD2-GFP transfected U2OS cells were lysed and processed for western blot with antibodies against GFP (to reveal SETD2-GFP), H3K36me3 and α-tubulin. Molecular weight markers (KDa) are shown on the left. **(D)** Live-cell images of SETD2-GFP dynamics were recorded upon laser-induced DNA damage of the indicated nuclear region of U2OS cells during 15min. **(E)** H3K36me3 was immunoprecipitated from MNase-digested U2OS cell extracts and each of the four nucleosomal histones was detected by immunobloting of the SDS-PAGE resolved complexes. **(F)** Nuclear co-immunoprecipitations before and 6 hours after NCS treatment were performed on U2OS cells using the indicated antibodies (I.P.: 53BP1 and H3K36me3). The Input lane represents total cell lysates and (-) denotes the negative control immunoprecipitation (beads only). Purified complexes were resolved by SDS-PAGE and blotted with antibodies against γH2AX or H3K36me3.

Figure 3. SETD2-independent DNA 5' end resection and RPA recruitment to DSBs
(A) Direct measurement of DNA 5' end resection at the *I-Sce*I site of the *GFP* gene in control and SETD2-depleted U2OS DR-GFP cells. The percentage of non-resected DNA at 250bp, 300bp, 350bp and 2200bp from the *I-Sce*I restriction site is shown. The percentage of DNA at each location was set to 100% in control cells. Means and standard deviations from five independent experiments using two distinct siRNAs targeting *SETD2* are shown. **(B)** Control and *SETD2* RNAi-depleted U2OS cells were challenged with NCS during 30min and chased in fresh media during the indicated time points. Western blot analysis was performed with antibodies against pRPA and total RPA. Molecular weight markers (KDa) are shown on the left. **(C)** Immunofluorescence of control and *SETD2* RNAi depleted U2OS cells before and 8h after NCS treatment was performed with antibodies against RPA and cyclin A. Dapi was added to the mounting medium to stain the DNA. Scale bars: 5μm. The graph shows the percentage of cells with more than 20 RPA foci. A minimum of 400 cells on each of three independent experiments was scored.

Figure 4. SETD2 promotes RAD51 recruitment to DSBs during DNA repair
Immunofluorescence of control and *SETD2* RNAi-depleted U2OS cells before and 8h after NCS treatment was performed with antibodies against BRCA1 **(A)** or RAD51 **(B)**. Cyclin A staining was performed in parallel. Dapi was added to the mounting medium to stain the DNA. Scale bars: 5μm. The graphs represent the average and standard deviations of the percentage of cells with BRCA1

or RAD51 foci after NCS treatment. A minimum of 500 cells from each of three individual experiments was scored for each experimental condition.

Figure 5. SETD2 is required for homologous recombination DNA repair
(A) The efficiency of homologous recombination in control and *SETD2* RNAi-depleted cells was investigated by measuring the fraction of GFP+ cells in the U2OS DR-GFP reporter assay. Means and standard deviations from five independent experiments using two distinct siRNAs targeting *SETD2* are shown. **(B)** Cell cycle progression of control and SETD2-depleted U2OS DR-GFP cells was obtained by flow cytometry analysis of propidium iodide staining.

Figure 6. ccRCC cells with inactivating mutations on *SETD2* show impaired DNA damage signalling
The H3K36me3 levels of *SETD2* wt and mutant ccRCC cells were inspected with an antibody against H3K36me3 by immunofluorescence **(A)**. **(B)** Immunofluorescence of *SETD2* wt and mutant ccRCC cells before and 30min after etoposide treatment for 15min was performed with an antibody against γH2AX. Dapi was added to the mounting medium to stain the DNA. Scale bars: 5μm. **(C** and **D)** Two *SETD2* wt (RCC-JW and Caki-2) and two *SETD2* mutant (RCC-MF and RCC-FG2) cell lines were challenged with etoposide during 15min and chased in fresh media during the indicated time points. Western blot analysis was performed with antibodies against the indicated proteins. Molecular weight markers (KDa) are shown on the left.

Figure 7. Repair of double strand breaks is compromised in *SETD2* mutant ccRCC cells
The amount of DNA damage immediately after induction of DSBs with etoposide and 3 and 6 hours after treatment was estimated by comet assay on *SETD2* wt and mutant ccRCC cells. Graphs depict the % of DNA in the tail of each individual comet. The horizontal solid lines represent the mean and 95% confidence intervals. At least 70 individual comets were analyzed for each time point.

Figure 8. SETD2 is required for p53 activation following DNA damage
(A) *SETD2* wt and mutant ccRCC cells were challenged with etoposide during 15min and chased in fresh media during the indicated time points. Western blot analysis was performed with antibodies against the proteins indicated on the right. *SETD2* wt ccRCC cells were depleted for SETD2 by RNAi, treated with etoposide **(B)**, NCS **(C)** or phleomycin **(D)** during the indicated periods of time and chased in fresh media. Western blot analysis was performed with antibodies against the proteins indicated on the right. Molecular weight markers (KDa) are shown on the left. Data are from one representative experiments of a total of three independent experiments performed with similar results.

Figure 9. SETD2 regulates the p53-dependent cell-cycle checkpoint and cell survival following DNA damage. (A) Control and *SETD2* RNAi-depleted cells were treated with 40μM of phleomycin to induce cell-cycle checkpoints. Cells were harvested at 0, 8 or 12 h after treatment, fixed and stained with propidium iodide, and analyzed by flow cytometry. Graphs show means and standard deviations of the percentage of cells at each phase of the cell cycle. Data are from 4 individual experiments. **(B)** Control and *SETD2* RNAi-depleted cells were treated with phleomycin at indicated concentrations and clonogenic survival was measured 10 days after treatment. Means and standard deviations from 6 individual cell cultures treated with each drug concentration are shown.

Figure 2 – figure supplement 1. Preparation of single-nucleosome extracts for the co-immunoprecipitation experiments. DNA was purified from MNase digested samples and resolved on a 1.8% agarose gel. The length of the DNA fragments is indicated on the left.

Figure 7 – figure supplement 1. Repair of double strand breaks in *SETD2* wt and mutant ccRCC cells. The amount of DNA damage 6 hours after etoposide treatment was estimated by comet assay on an additional pair of *SETD2* wt (Caki-2) and mutant (RCC-FG2) cells. Graphs depict the % of DNA in the tail of each individual comet. The horizontal solid lines represent the mean and 95% confidence intervals.

Table 1. Sequence of primers used in this study.

Gene Name	Primer Designation	Primer Sequence
*I-Sce*I *Flank*	Flank_Fw	GAG CAG GAA CCT GAG GAG
	Flank_Rv	GCC GTA GGT ATT ACC CTG
*I-Sce*I *250bp*	250bp_Fw	CAT GCC CGA AGG CTA CGT
	250bp_Rv	CGG CGC GGG TCT TGT A
*I-Sce*I *300bp*	300bp_Fw	CTT CTT CAA GGA CGA CGG C
	300bp_Rv	GTA GTT GTA CTC CAG CTT GTG
*I-Sce*I *350bp*	350bp_Fw	CTA CAG CTC CTG GGC AAC
	350bp_Rv	CTT CGG CAC CTT TCT CTT C
*I-Sce*I *2200bp*	2200bp_Fw	CGC GAC GTC TGT CGA GAA G
	2200bp_Rv	GCC GAT GCA AAG TGC CGA TA
GAPDH	GAPDH_Fw	GAA GGT GGA GGT CGG AGT C
	GAPDH_Rv	GAA GAT GGT GAT GGG ATT TC

Figure 1

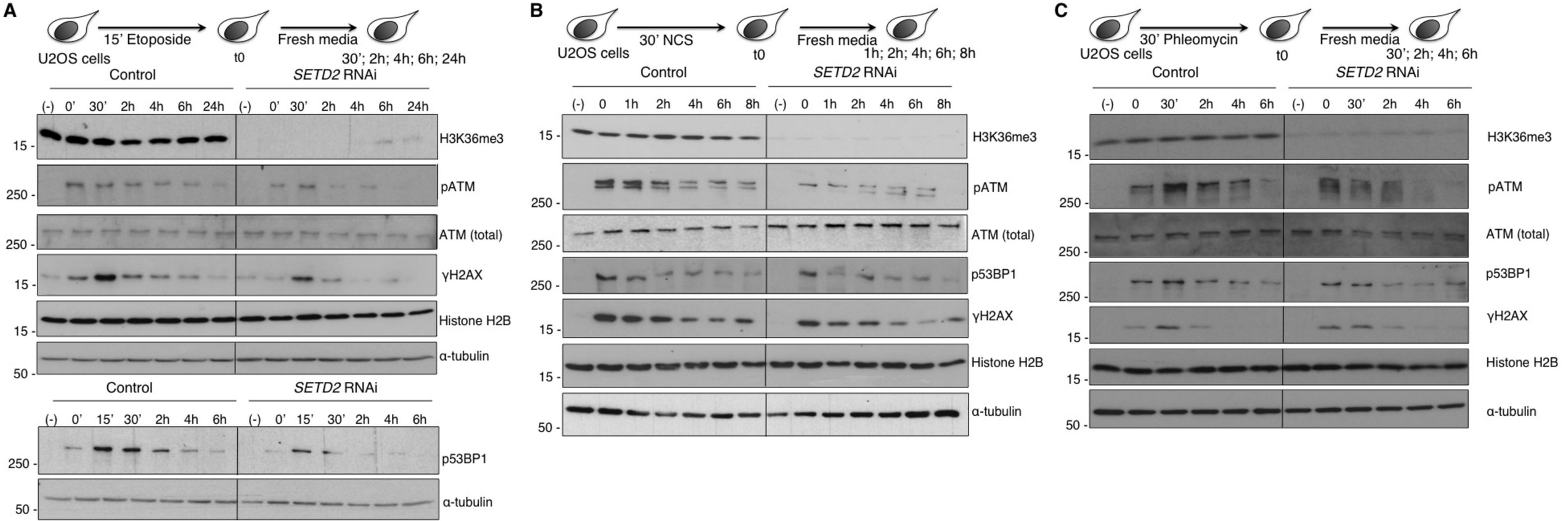
A
U2OS cells
15' Etoposide
t0
Fresh media
30'; 2h; 4h; 6h; 24h
Control
SETD2 RNAi
(-) 0' 30' 2h 4h 6h 24h
H3K36me3
pATM
ATM (total)
γH2AX
Histone H2B
α-tubulin
(-) 0' 15' 30' 2h 4h 6h
p53BP1
B
U2OS cells
30' NCS
t0
Fresh media
1h; 2h; 4h; 6h; 8h
(-) 0 1h 2h 4h 6h 8h
p53BP1
C
U2OS cells
30' Phleomycin
t0
Fresh media
30'; 2h; 4h; 6h
(-) 0 30' 2h 4h 6h

Figure 2

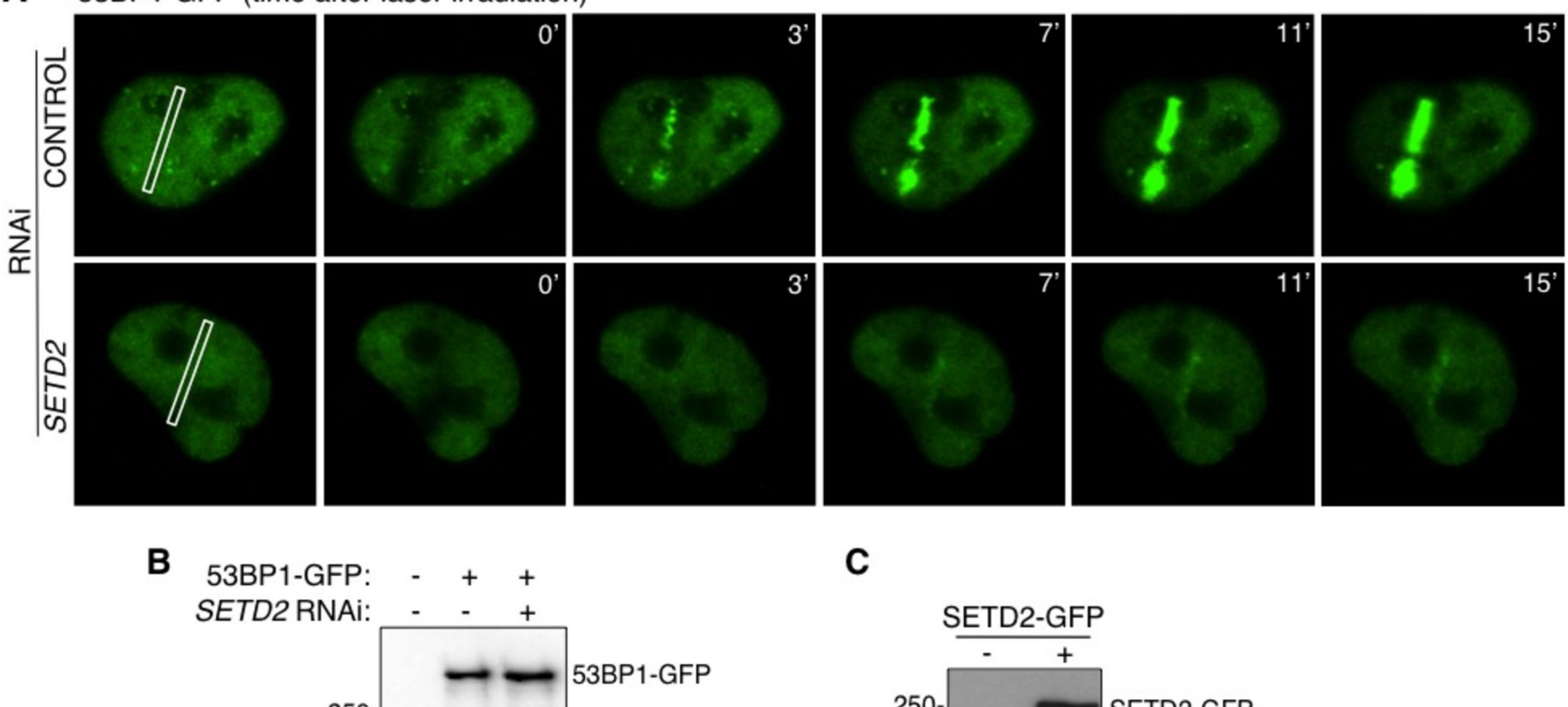
A
53BP1-GFP (time after laser irradiation)
RNAi
CONTROL
SETD2
0'
3'
7'
11'
15'

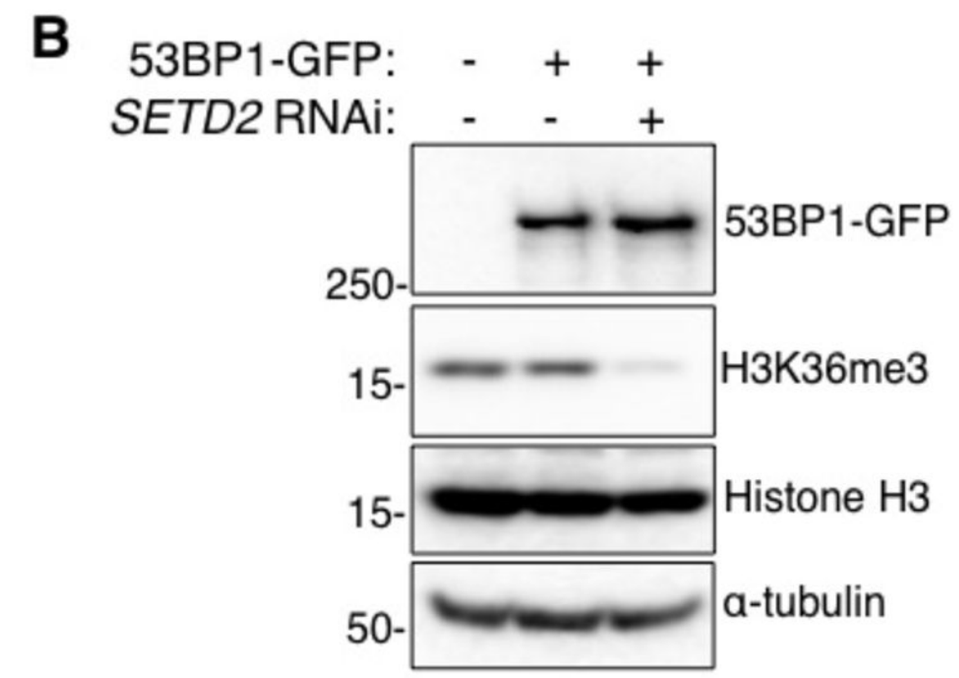
B
53BP1-GFP: - + +
SETD2 RNAi: - - +
250-
53BP1-GFP
15-
H3K36me3
15-
Histone H3
50-
α-tubulin

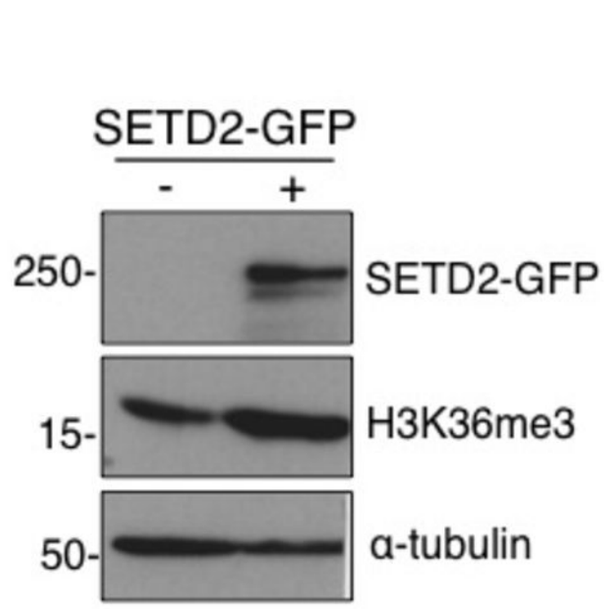
C
SETD2-GFP
- +
250-
SETD2-GFP
15-
H3K36me3
50-
α-tubulin

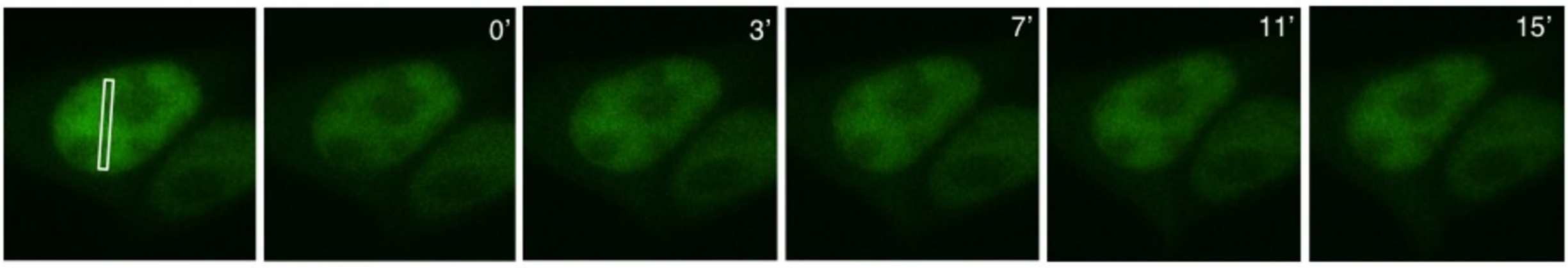
D
SETD2-GFP (time after laser irradiation)
0'
3'
7'
11'
15'

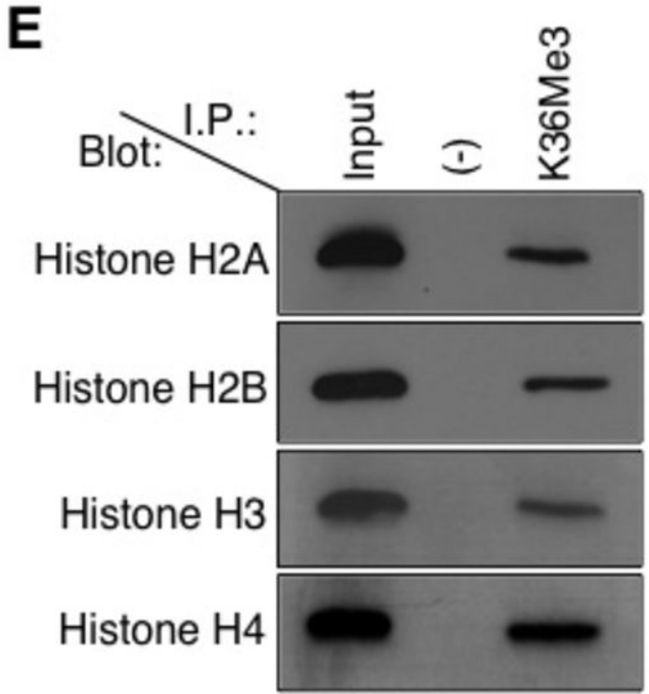
E
I.P.:
Blot:
Input
(-)
K36Me3
Histone H2A
Histone H2B
Histone H3
Histone H4

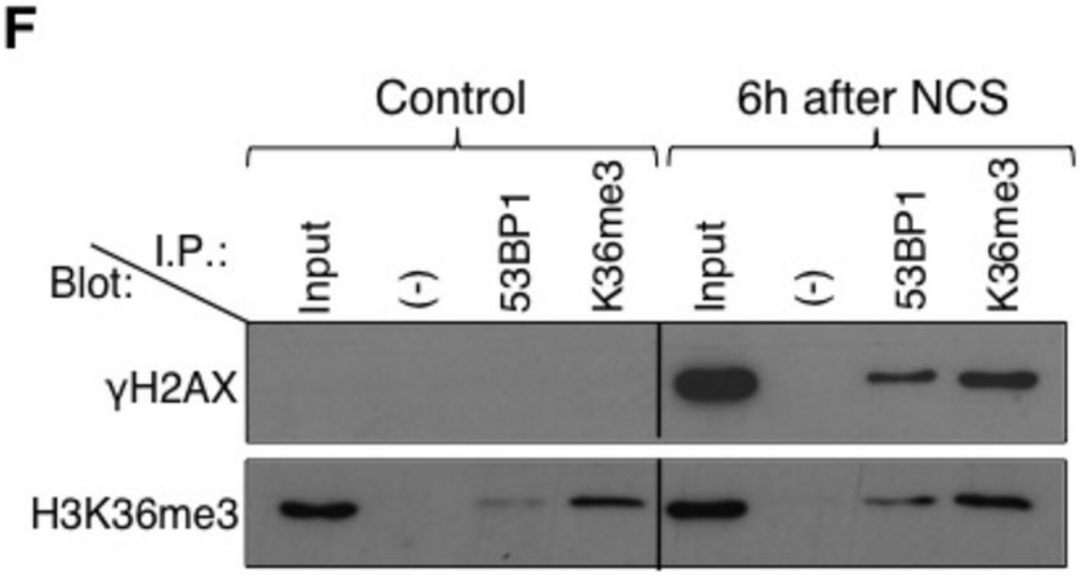
F
Control
6h after NCS
I.P.:
Blot:
Input
(-)
53BP1
K36me3
Input
(-)
53BP1
K36me3
γH2AX
H3K36me3

Figure 3

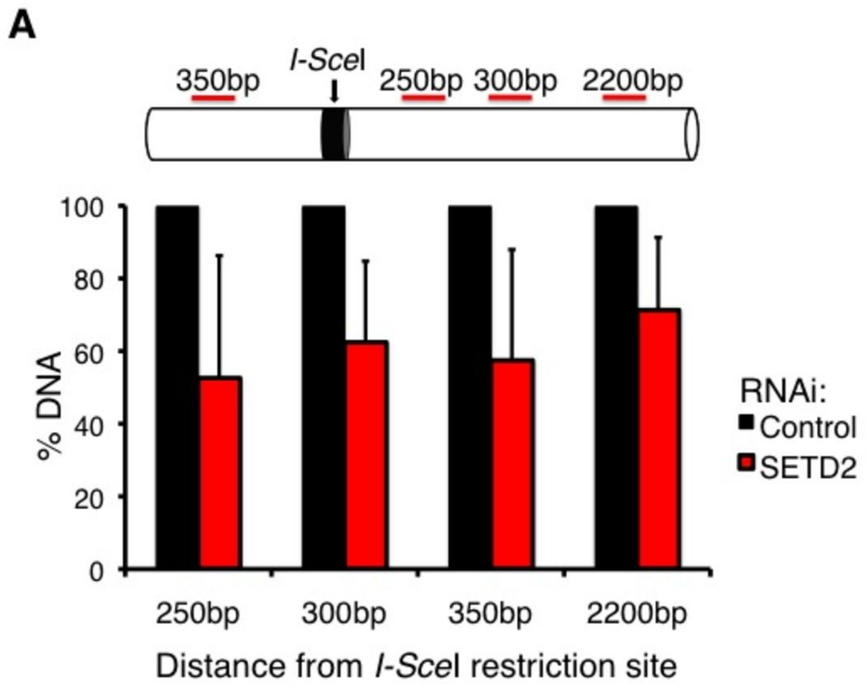
A
350bp
I-SceI
250bp
300bp
2200bp
100
80
60
40
20
0
% DNA
250bp
300bp
350bp
2200bp
Distance from I-SceI restriction site
RNAi:
Control
SETD2

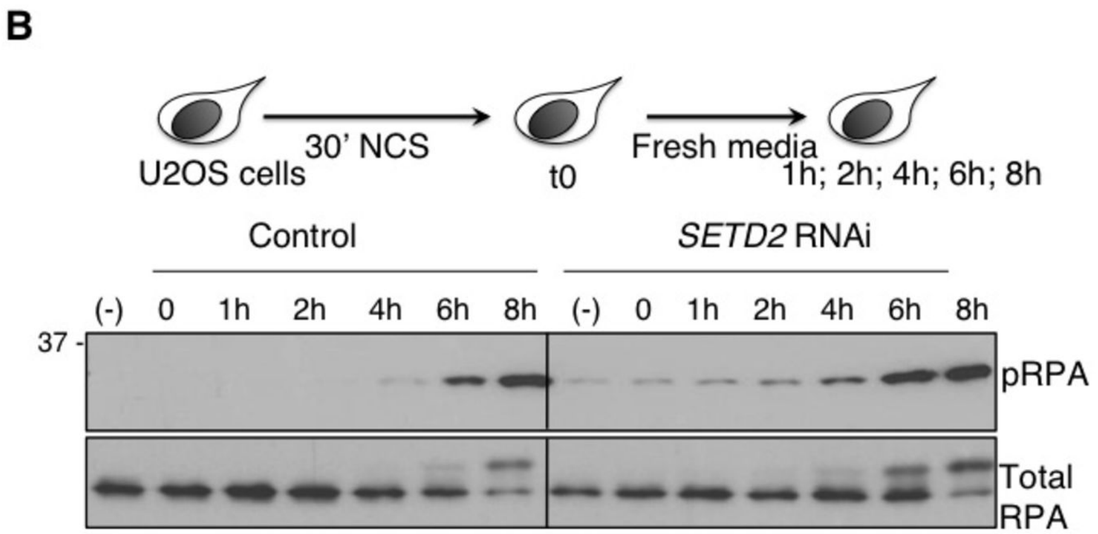
B
U2OS cells
30' NCS
t0
Fresh media
1h; 2h; 4h; 6h; 8h
Control
SETD2 RNAi
(-) 0 1h 2h 4h 6h 8h (-) 0 1h 2h 4h 6h 8h
37 -
pRPA
Total RPA

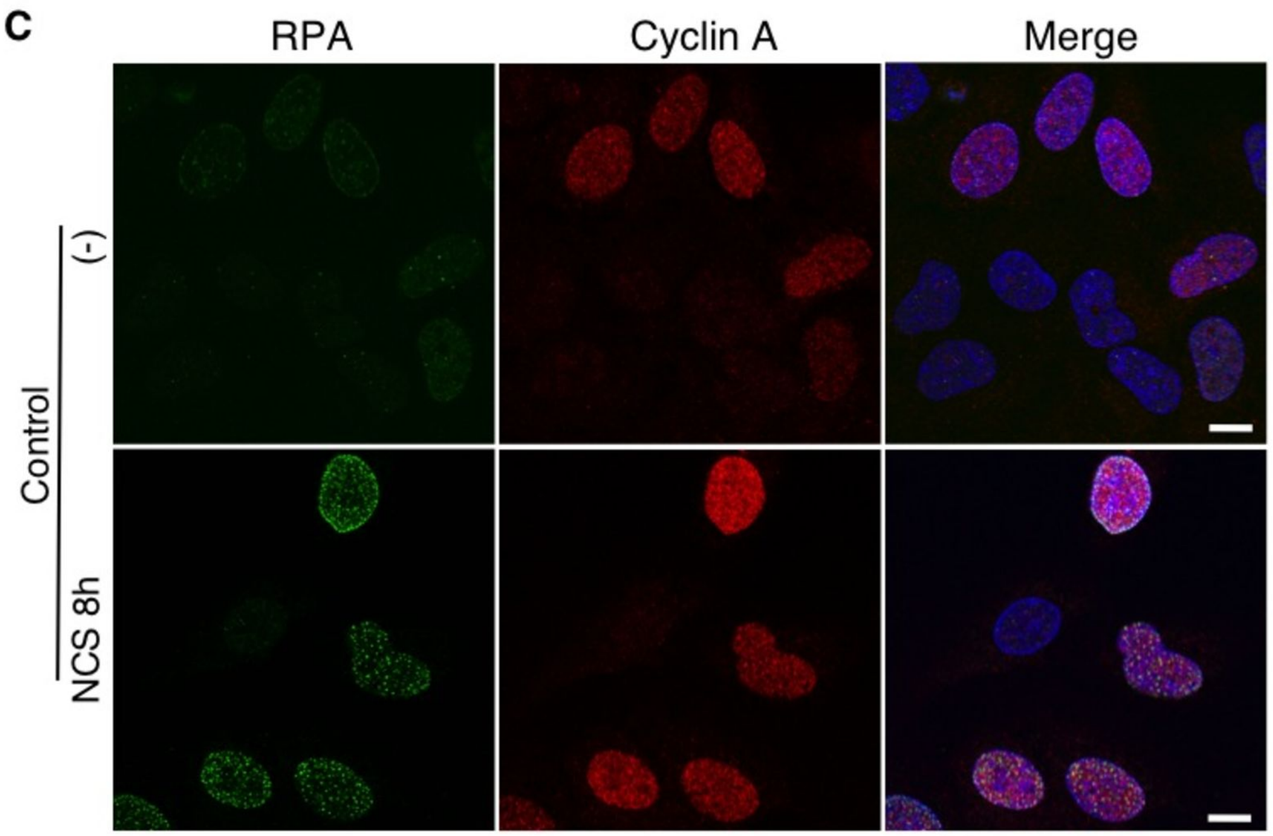
C
RPA
Cyclin A
Merge
Control
SETD2 RNAi
(-)
NCS 8h

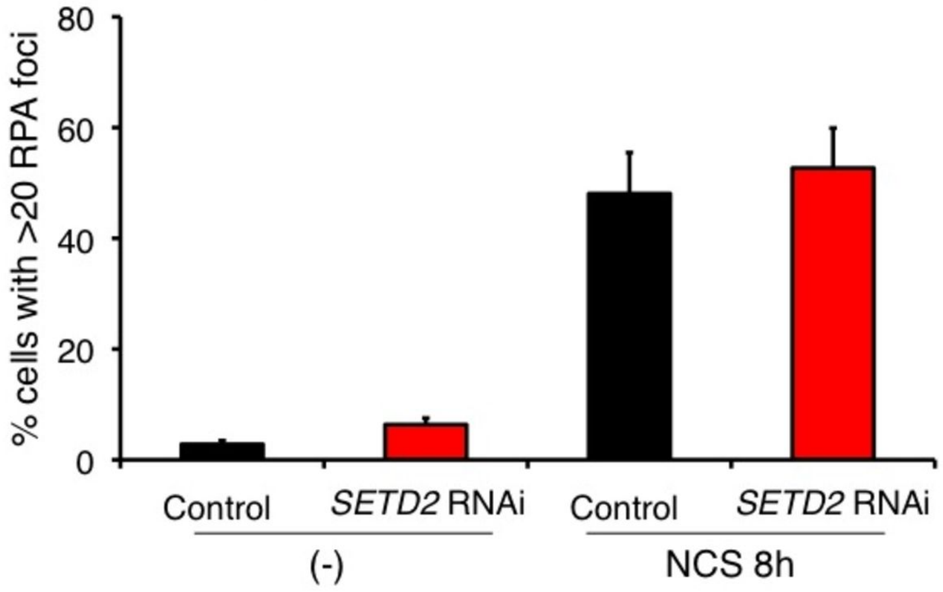
80
60
40
20
0
% cells with >20 RPA foci
Control
SETD2 RNAi
Control
SETD2 RNAi
(-)
NCS 8h

Figure 4

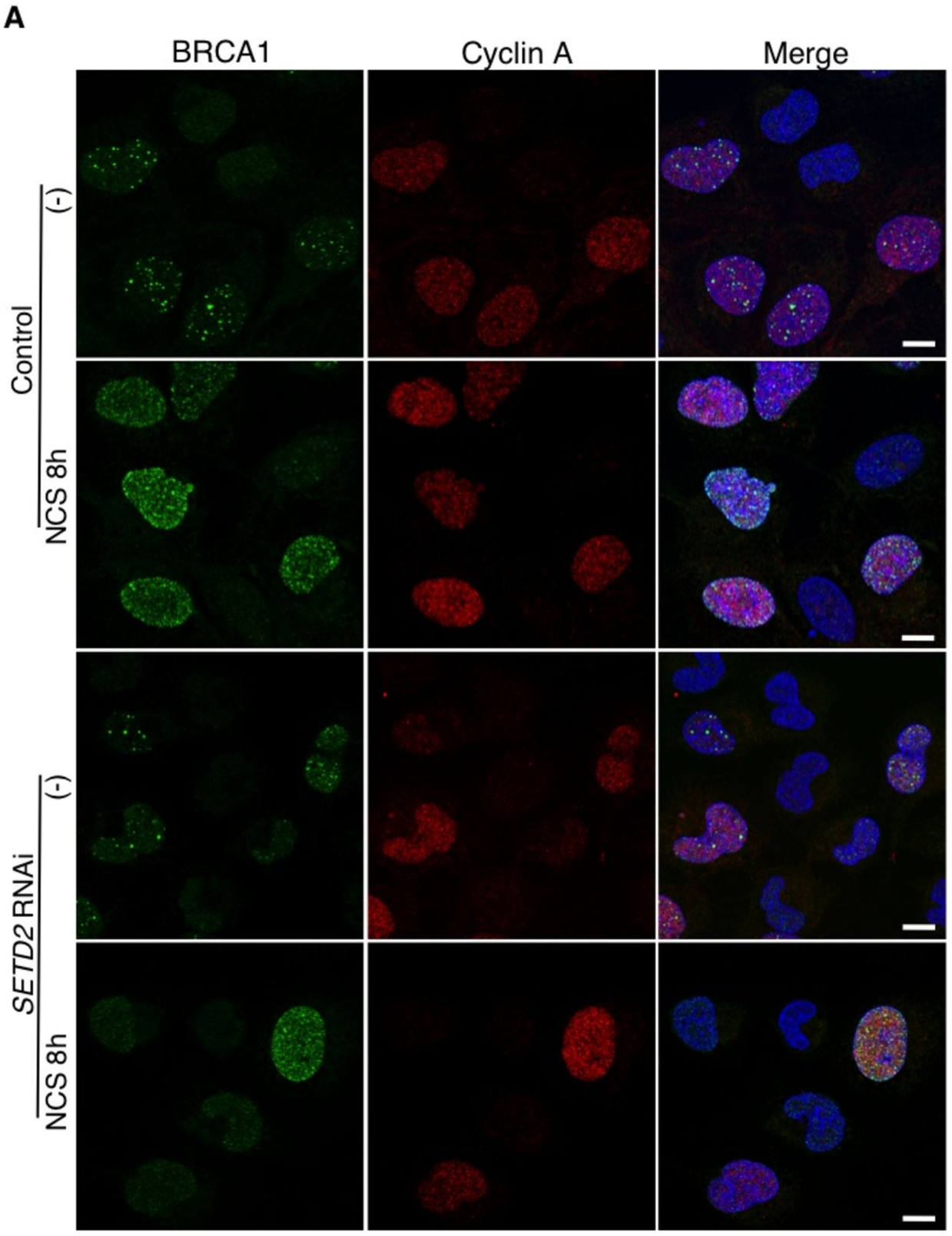
A
BRCA1
Cyclin A
Merge
Control
(-)
NCS 8h
SETD2 RNAi
(-)
NCS 8h

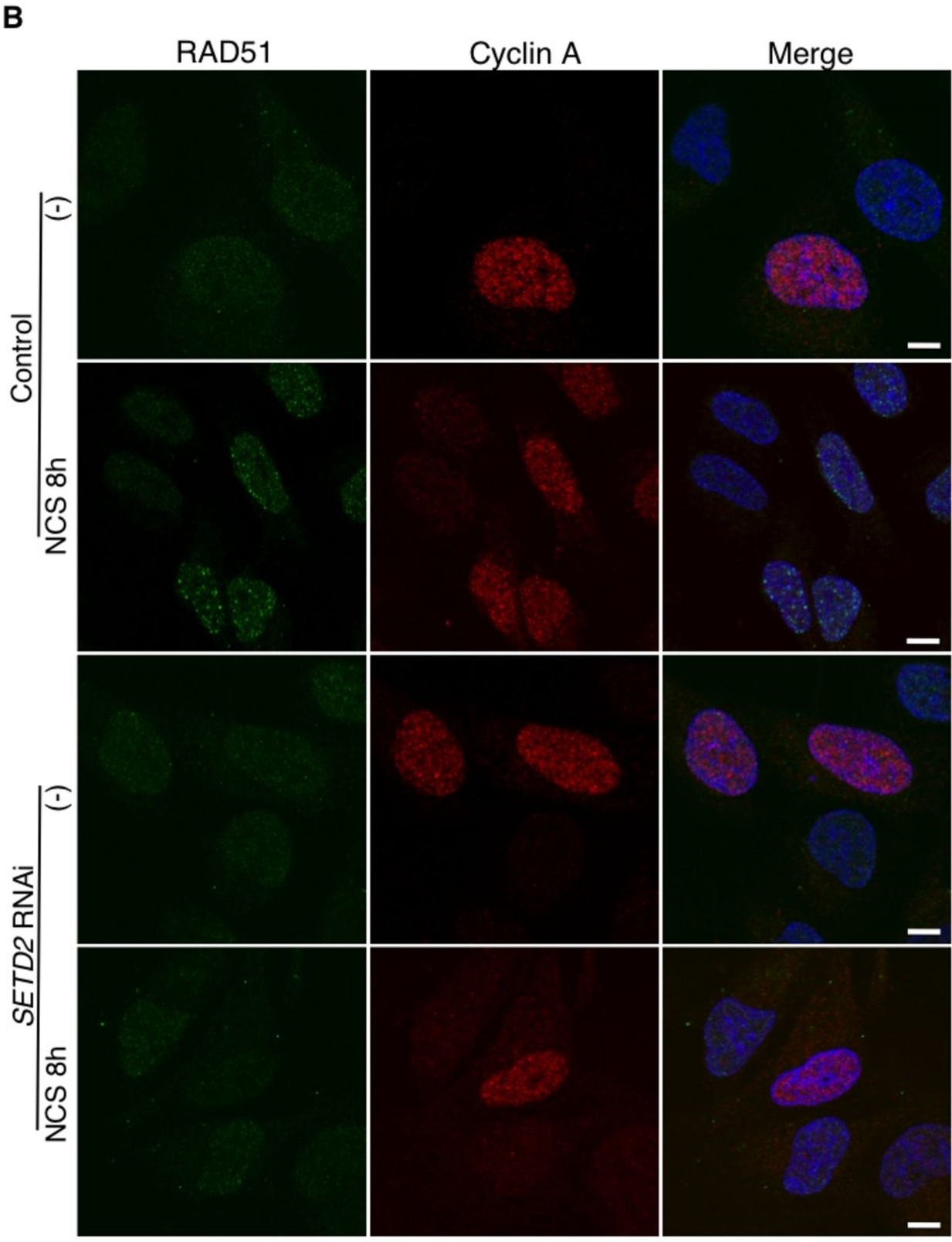
B
RAD51
Cyclin A
Merge
Control
(-)
NCS 8h
SETD2 RNAi
(-)
NCS 8h

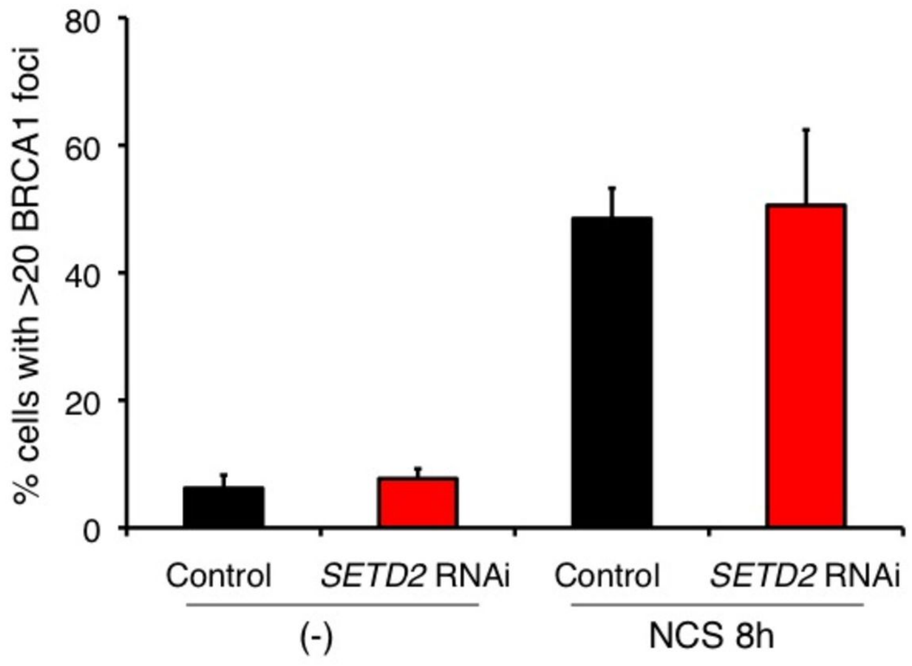
% cells with >20 BRCA1 foci
80
60
40
20
0
Control
SETD2 RNAi
Control
SETD2 RNAi
(-)
NCS 8h

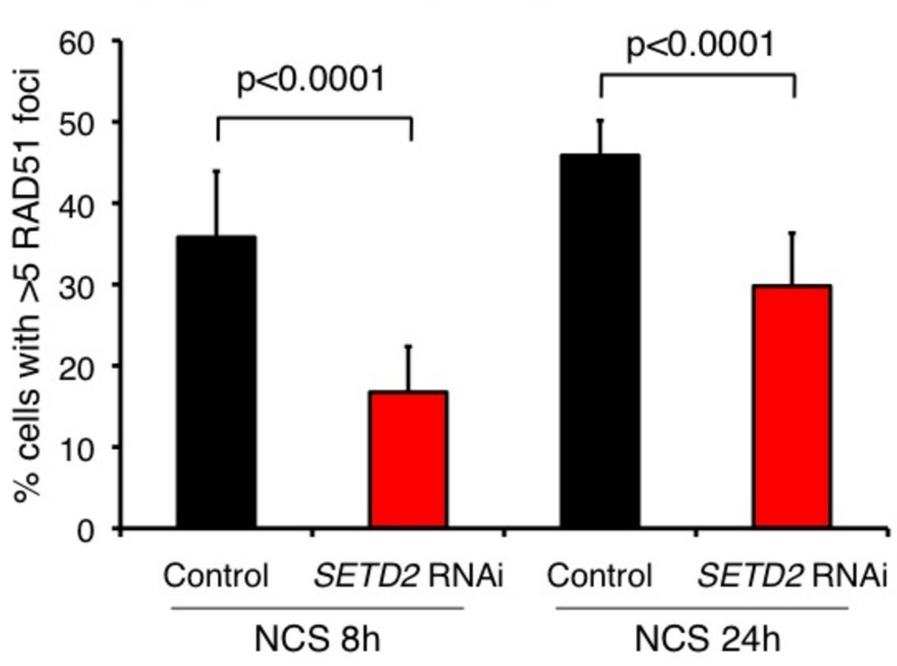
% cells with >5 RAD51 foci
60
50
40
30
20
10
0
p<0.0001
p<0.0001
Control
SETD2 RNAi
Control
SETD2 RNAi
NCS 8h
NCS 24h

Figure 5

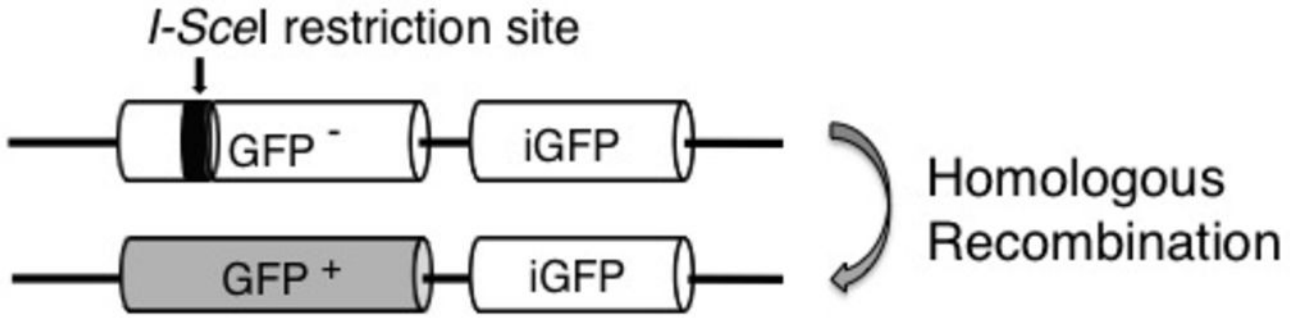
I-SceI restriction site
GFP -
iGFP
GFP +
iGFP
Homologous
Recombination

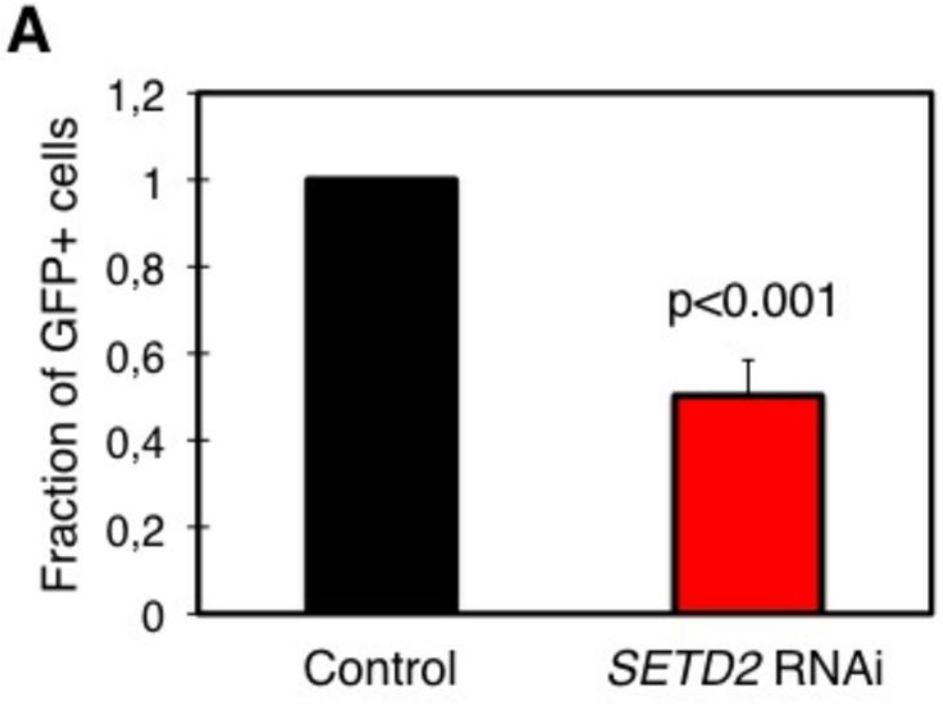
A
Fraction of GFP+ cells
1,2
1
0,8
0,6
0,4
0,2
0
p<0.001
Control
SETD2 RNAi

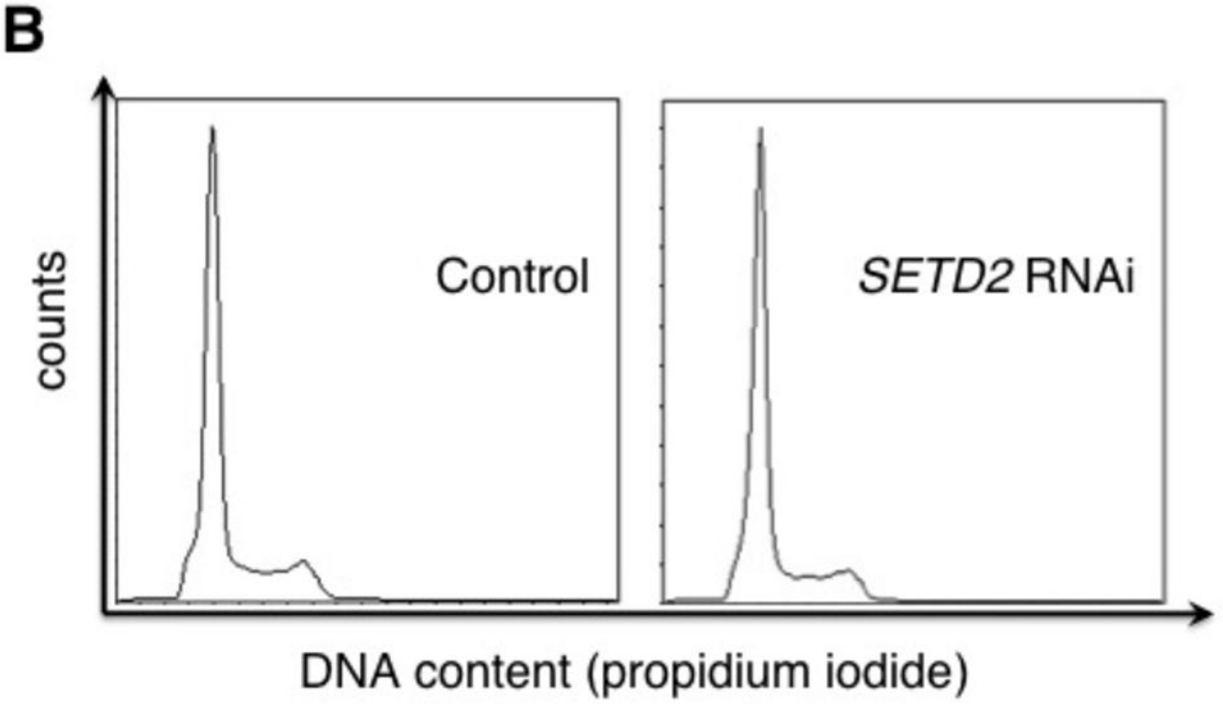
B
counts
Control
SETD2 RNAi
DNA content (propidium iodide)

Figure 6

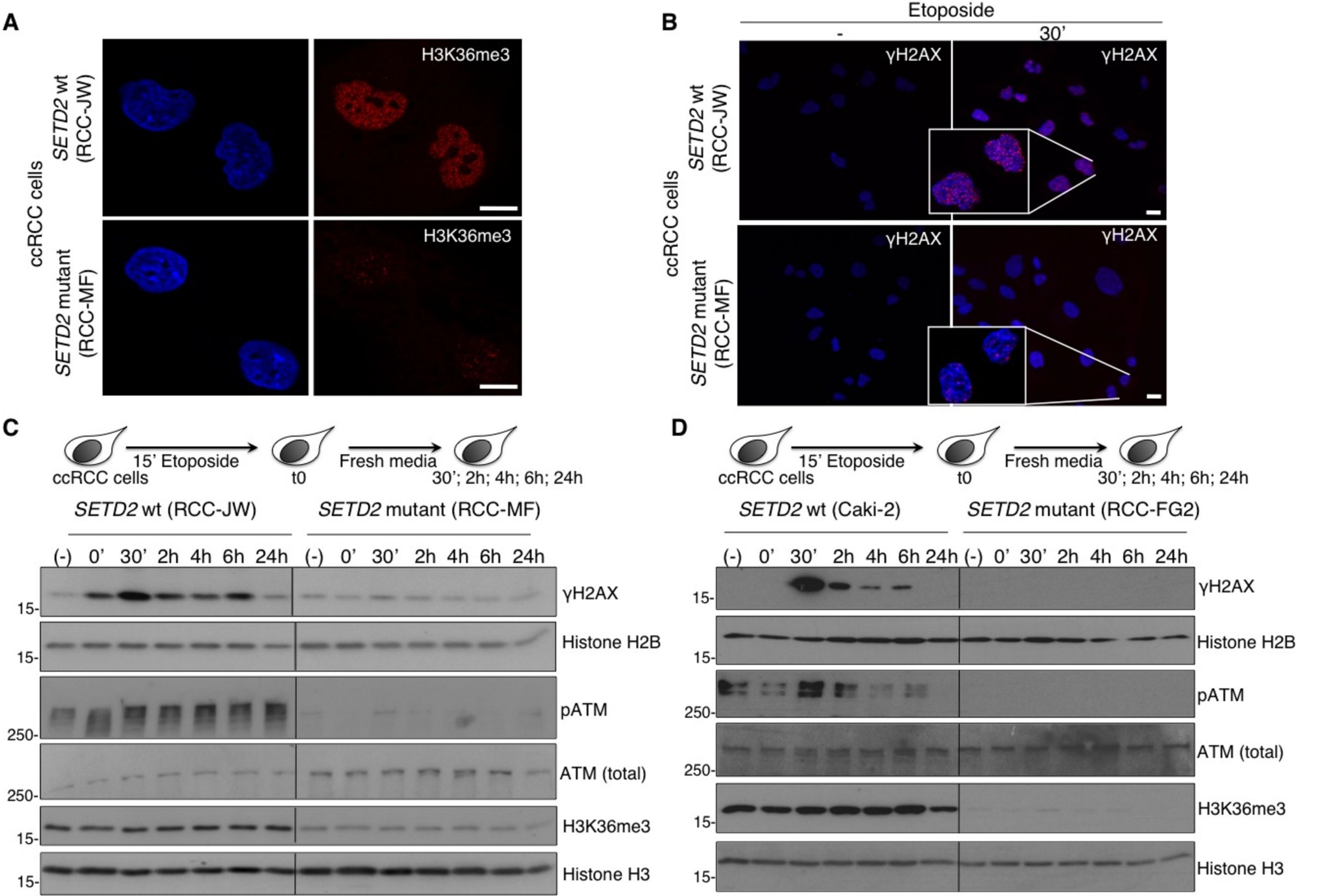
A
ccRCC cells
SETD2 wt (RCC-JW)
SETD2 mutant (RCC-MF)
H3K36me3
H3K36me3
B
Etoposide
-
30'
ccRCC cells
SETD2 wt (RCC-JW)
SETD2 mutant (RCC-MF)
γH2AX
γH2AX
γH2AX
γH2AX
C
15' Etoposide
ccRCC cells
t0
Fresh media
30'; 2h; 4h; 6h; 24h
SETD2 wt (RCC-JW)
SETD2 mutant (RCC-MF)
(-) 0' 30' 2h 4h 6h 24h (-) 0' 30' 2h 4h 6h 24h
15-
γH2AX
15-
Histone H2B
250-
pATM
250-
ATM (total)
15-
H3K36me3
15-
Histone H3
D
15' Etoposide
ccRCC cells
t0
Fresh media
30'; 2h; 4h; 6h; 24h
SETD2 wt (Caki-2)
SETD2 mutant (RCC-FG2)
(-) 0' 30' 2h 4h 6h 24h (-) 0' 30' 2h 4h 6h 24h
15-
γH2AX
15-
Histone H2B
250-
pATM
250-
ATM (total)
15-
H3K36me3
15-
Histone H3

Figure 7

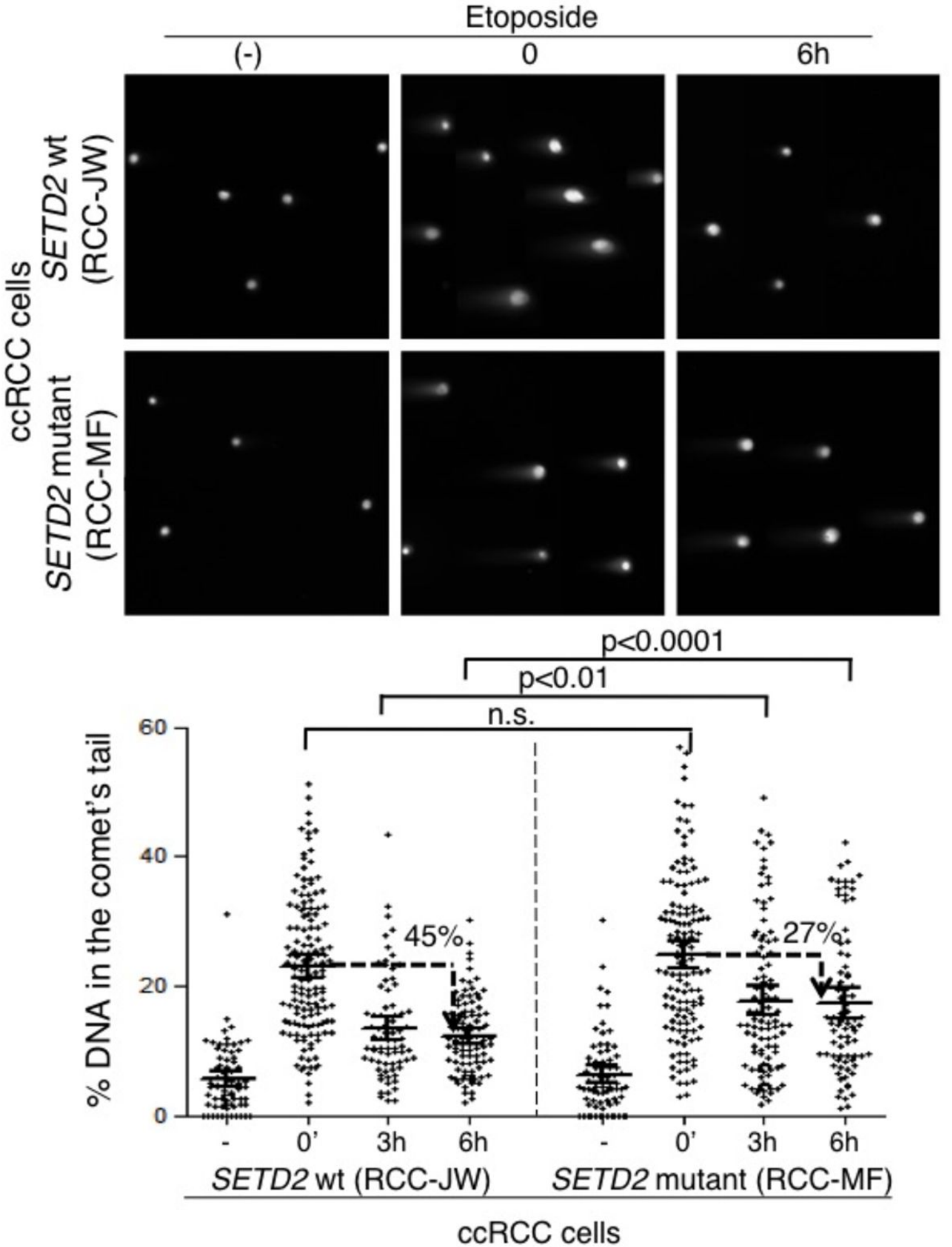
Etoposide
(-)
0
6h
ccRCC cells
SETD2 wt (RCC-JW)
SETD2 mutant (RCC-MF)
p<0.0001
p<0.01
n.s.
% DNA in the comet's tail
60
40
20
0
45%
27%
-
0'
3h
6h
-
0'
3h
6h
SETD2 wt (RCC-JW)
SETD2 mutant (RCC-MF)
ccRCC cells

Figure 8

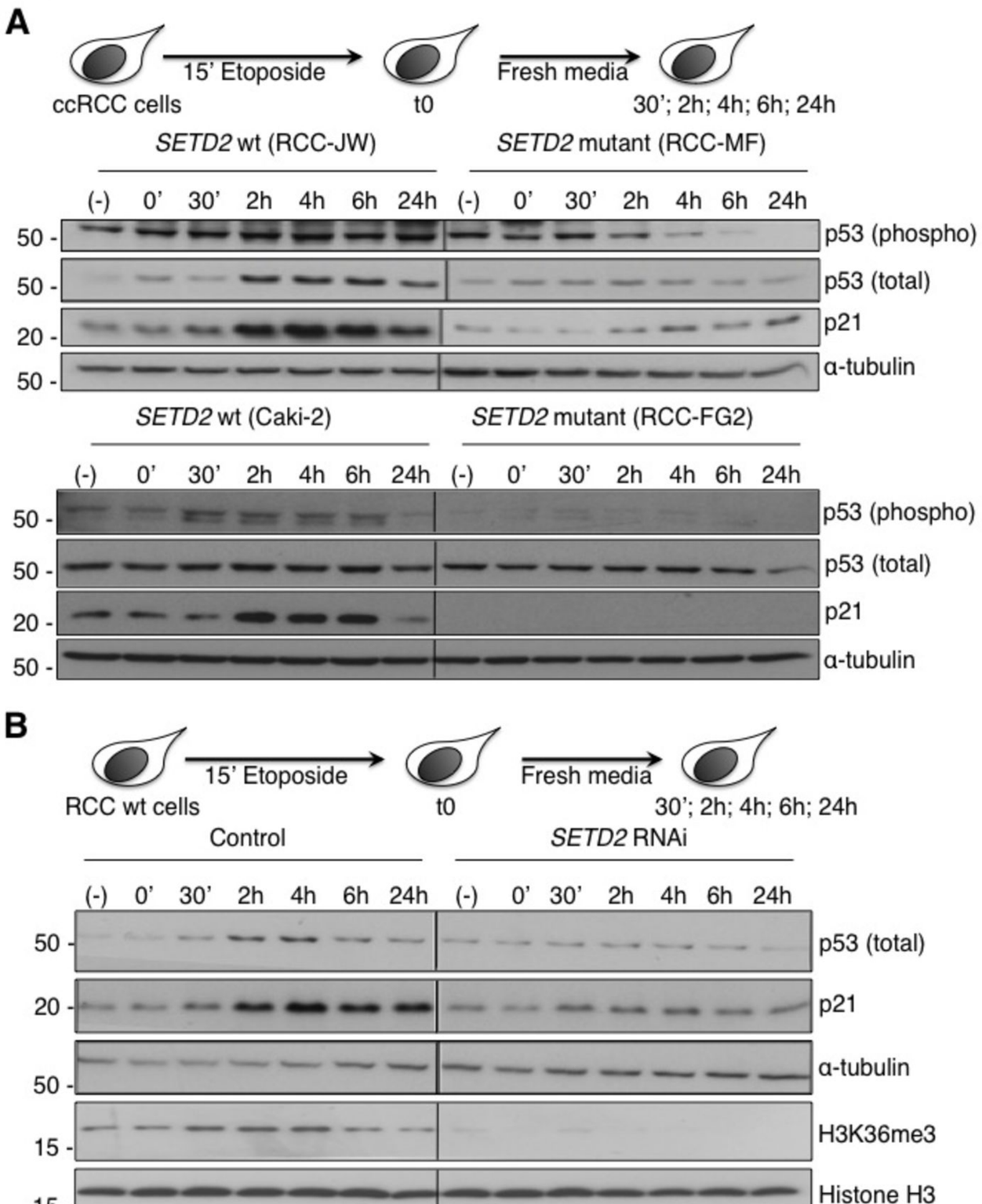
A
15' Etoposide
ccRCC cells
t0
Fresh media
30'; 2h; 4h; 6h; 24h
SETD2 wt (RCC-JW)
SETD2 mutant (RCC-MF)
(-) 0' 30' 2h 4h 6h 24h
p53 (phospho)
p53 (total)
p21
α-tubulin
SETD2 wt (Caki-2)
SETD2 mutant (RCC-FG2)
B
15' Etoposide
RCC wt cells
t0
Fresh media
30'; 2h; 4h; 6h; 24h
Control
SETD2 RNAi
(-) 0' 30' 2h 4h 6h 24h
p53 (total)
p21
α-tubulin
H3K36me3
Histone H3
C
30' NCS
RCC wt cells
t0
Fresh media
1h; 2h; 4h; 6h; 8h
Control
SETD2 RNAi
(-) 0 1h 2h 4h 6h 8h
p53 (total)
p21
α-tubulin
H3K36me3
Histone H3
D
30' Phleomycin
RCC wt cells
t0
Fresh media
30'; 2h; 4h; 6h
Control
SETD2 RNAi
(-) 0 30' 2h 4h 6h
p53 (total)
p21
α-tubulin
H3K36me3
Histone H3

Figure 9

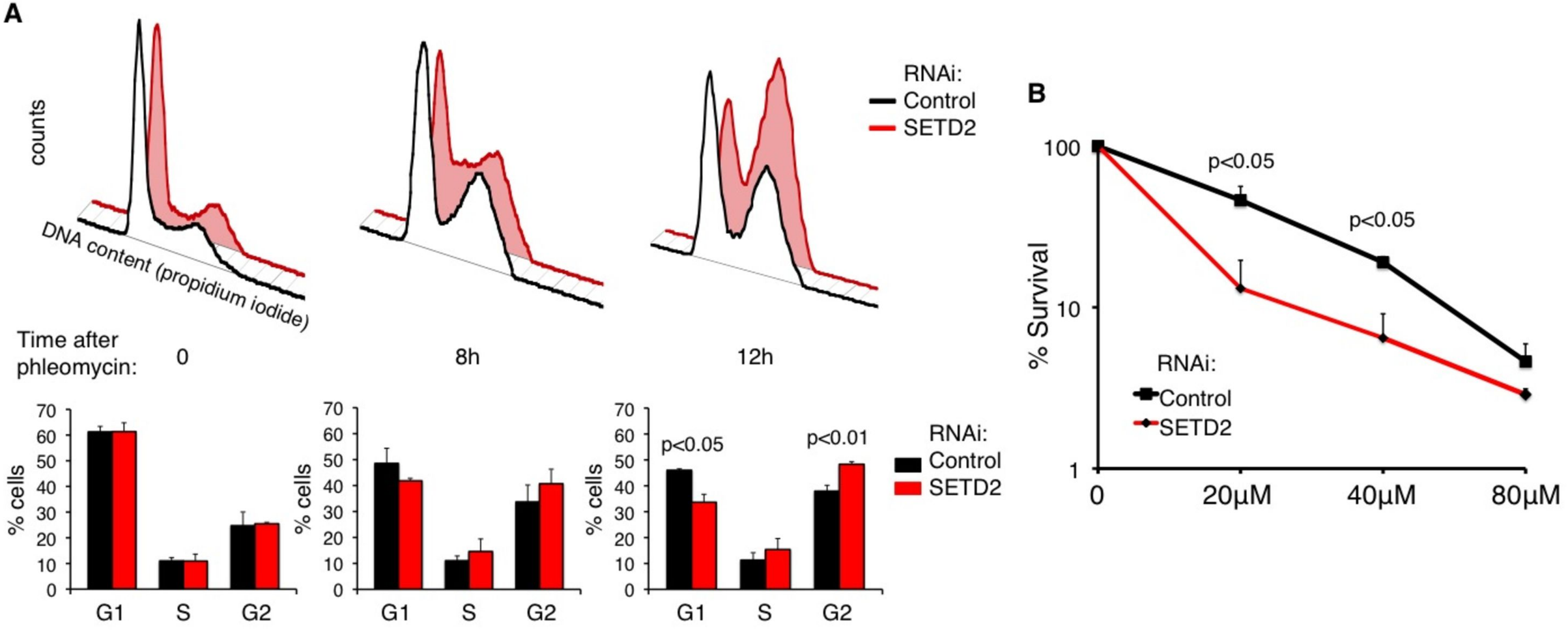
A
counts
DNA content (propidium iodide)
RNAi:
Control
SETD2
Time after phleomycin:
0
8h
12h
% cells
G1
S
G2
p<0.05
p<0.01
B
% Survival
p<0.05
p<0.05
RNAi:
Control
SETD2
0
20μM
40μM
80μM